Bioactive Materials 42 (2024) 241–256

Contents lists available at ScienceDirect

Bioactive Materials

journal homepage: www.keaipublishing.com/en/journals/bioactive-materials

ECM-mimicking composite hydrogel for accelerated vascularized bone regeneration

Guanglong Li [a,1], Fei Gao [b,1], Donglei Yang [b], Lu Lin [a], Weijun Yu [a], Jiaqi Tang [a], Ruhan Yang [a], Min Jin [a], Yuting Gu [a], Pengfei Wang [b,**], Eryi Lu [a,*]

[a] Department of Stomatology, Renji Hospital, Shanghai Jiao Tong University School of Medicine, 160 Pujian Road, Shanghai, 200127, China
[b] Institute of Molecular Medicine, Shanghai Key Laboratory for Nucleic Acid Chemistry and Nanomedicine, Renji Hospital, Shanghai Jiao Tong University School of Medicine, 160 Pujian Road, Shanghai, 200127, China

ARTICLE INFO

Keywords:
Composite hydrogel
DNA hydrogel
Stress relaxation
Osteogenesis
Vascularization

ABSTRACT

Bioactive hydrogel materials have great potential for applications in bone tissue engineering. However, fabrication of functional hydrogels that mimic the natural bone extracellular matrix (ECM) remains a challenge, because they need to provide mechanical support and embody physiological cues for angiogenesis and osteogenesis. Inspired by the features of ECM, we constructed a dual-component composite hydrogel comprising interpenetrating polymer networks of gelatin methacryloyl (GelMA) and deoxyribonucleic acid (DNA). Within the composite hydrogel, the GelMA network serves as the backbone for mechanical and biological stability, whereas the DNA network realizes dynamic capabilities (e.g., stress relaxation), thereby promoting cell proliferation and osteogenic differentiation. Furthermore, functional aptamers (Apt19S and AptV) are readily attached to the DNA network to recruit bone marrow mesenchymal stem cells (BMSCs) and achieve sustained release of loaded vascular endothelial growth factor towards angiogenesis. Our results showed that the composite hydrogel could facilitate the adhesion of BMSCs, promote osteogenic differentiation by activating focal adhesion kinase (FAK)/phosphatidylinositol 3-kinase (PI3K)/protein kinase B (Akt)/β-Catenin signaling pathway, and eventually enhance vascularized bone regeneration. This study shows that the multifunctional composite hydrogel of GelMA and DNA can successfully simulate the biological functions of natural bone ECM and has great potential for repairing bone defects.

1. Introduction

Bone defects caused by tumor, injuries and other bone diseases can lead to severe trauma and dysfunction. The repair of bone defect remains a considerable challenge for surgeons [1]. Although tissue engineering biomaterials have made significant progress in bone healing treatments, their therapeutic effect is not ideal [2,3]. Bone healing is a complex physiological process that needs the coordinated occurrence of angiogenesis and osteogenesis [4,5]. Biomaterials implanted in bone defects should provide mechanical support as scaffolds, and imitate the natural bone extracellular matrix (ECM) to exert multiple functions [6]. Natural bone ECM can attract osteogenic-related cells and improve cell migration to bone defect areas [7]. Owing to its mechanical property of viscoelasticity, natural bone ECM is dynamic and provides mechanical signals to promote cell adhesion, proliferation and osteogenic differentiation [8–10]. Meanwhile, natural bone ECM can store growth factors secreted by cells and continuously release factors to promote vascular growth to support bone formation [11–13]. Therefore, biomaterials with the following characteristics and functions may better simulate natural bone ECM: 1) suitable mechanical strength, 2) recruitment of osteogenic-related cells, 3) dynamic property of viscoelasticity, 4) sustainable release of factors to promote vascularization.

Hydrogels based on crosslinked polymer chains are highly aqueous three-dimensional (3D) network materials [14]. Because of their unique water-rich nature and plasticity, hydrogels can be easily implanted in different forms of bone defects and have been widely studied and

Peer review under responsibility of KeAi Communications Co., Ltd.
* Corresponding author.
** Corresponding author.
E-mail addresses: pengfei.wang@sjtu.edu.cn (P. Wang), lueryi222@outlook.com (E. Lu).
[1] These authors contributed equally: Guanglong Li, Fei Gao.

https://doi.org/10.1016/j.bioactmat.2024.08.035
Received 15 May 2024; Received in revised form 7 August 2024; Accepted 27 August 2024

utilized in the field of bone regeneration [15–17]. Compared with single-component hydrogels, multi-component composite hydrogels have been considered to better mimic ECM features in the complicated microenvironment of bone defects [18]. Gelatin methacryloyl (GelMA) possesses the advantages of gelatin such as excellent biocompatibility, good mechanical characteristics and suitable degradability, and it plays the role of mechanical support in the initial stage of bone repair and gradually degrades with the growth of new tissues in the later stage [19]. However, current research demonstrates that pure GelMA has insufficient osteogenic effects, and does not provide a coordinated occurrence of vascularization and bone formation [20,21]. Natural bone ECM is viscoelastic and exhibits rapid stress relaxation. An increasing number of reports have indicated that rapid stress relaxation promotes cell growth and differentiation [8,22,23]. As a type of covalent cross-linking hydrogel, GelMA is robust and elastic, presenting fewer stress relaxation properties, which limits cell proliferation and differentiation [24]. In addition, unlike natural bone ECM, individual ingredients of gelatin are not equipped with the ability to recruit bone marrow mesenchymal stem cells (BMSCs). Furthermore, when treated as a drug delivery system, GelMA hydrogel poorly incorporates or retains growth factors; thus, it exhibits a kinetic phenomenon of "burst release" and most of the growth factors are released over the initial period [25,26]. The "burst release" phenomenon limits the application of GelMA hydrogel in carrying growth factors to promote vascularization during bone formation.

Deoxyribonucleic acid (DNA), previously considered a genetic substance, has evolved into an excellent building block for preparing biomedical materials for tissue regeneration [27,28]. As a class of peculiar functional short nucleic acid, aptamers can serve as novel recognition ligands to bind with their targets with high affinity and specificity. With the different tertiary structures, aptamers can recognize various kinds of targets, including metal ions, proteins and even cells [29,30]. In the field of bone regeneration, aptamers with definite recognition have been broadly used. For example, Apt19S was proved to label multipotent stem cells such as MSCs. Cell-free scaffold materials decorated with Apt19S have been confirmed to recognize and recruit *in situ* BMSCs from bone marrow environment efficiently [31,32]. In order to enhance the vascularization during the growth of new bone, scaffold materials modified with vascular endothelial growth factor (VEGF) aptamers were fabricated to improve VEGF release kinetics and made the scaffold a desirable VEGF factor carrier [33,34]. In addition, due to its precise and reversible complementary base pair crosslinking, DNA has emerged as a popular material for the preparation of smart hydrogels [35,36]. Recently, some studies have reported that natural salmon DNA can rehybridize to form adaptable hydrogels for bone regeneration, by heating and cooling [37,38]. In addition to salmon DNA, Athanasiadou et al. reported a pure DNA 3D hydrogel that could repair bone defects and suggested that artificially designed sequences of DNA strands could form DNA self-assembly hydrogels in a simple way [39]. These findings inspired us to develop programmable DNA strands armed with aptamers to realize multifunctional dynamic hydrogel networks for bone tissue engineering. Although several advantages have been confirmed, the application of pure DNA hydrogels for bone formation is still limited due to insufficient mechanical strength and relatively fast degradation [36,40]. Therefore, designed DNA structures can be combined with GelMA to create an ECM-mimicking composite hydrogel.

In this study, we fabricated a composite hydrogel based on GelMA and DNA backbone modified with aptamers to restore the multilevel

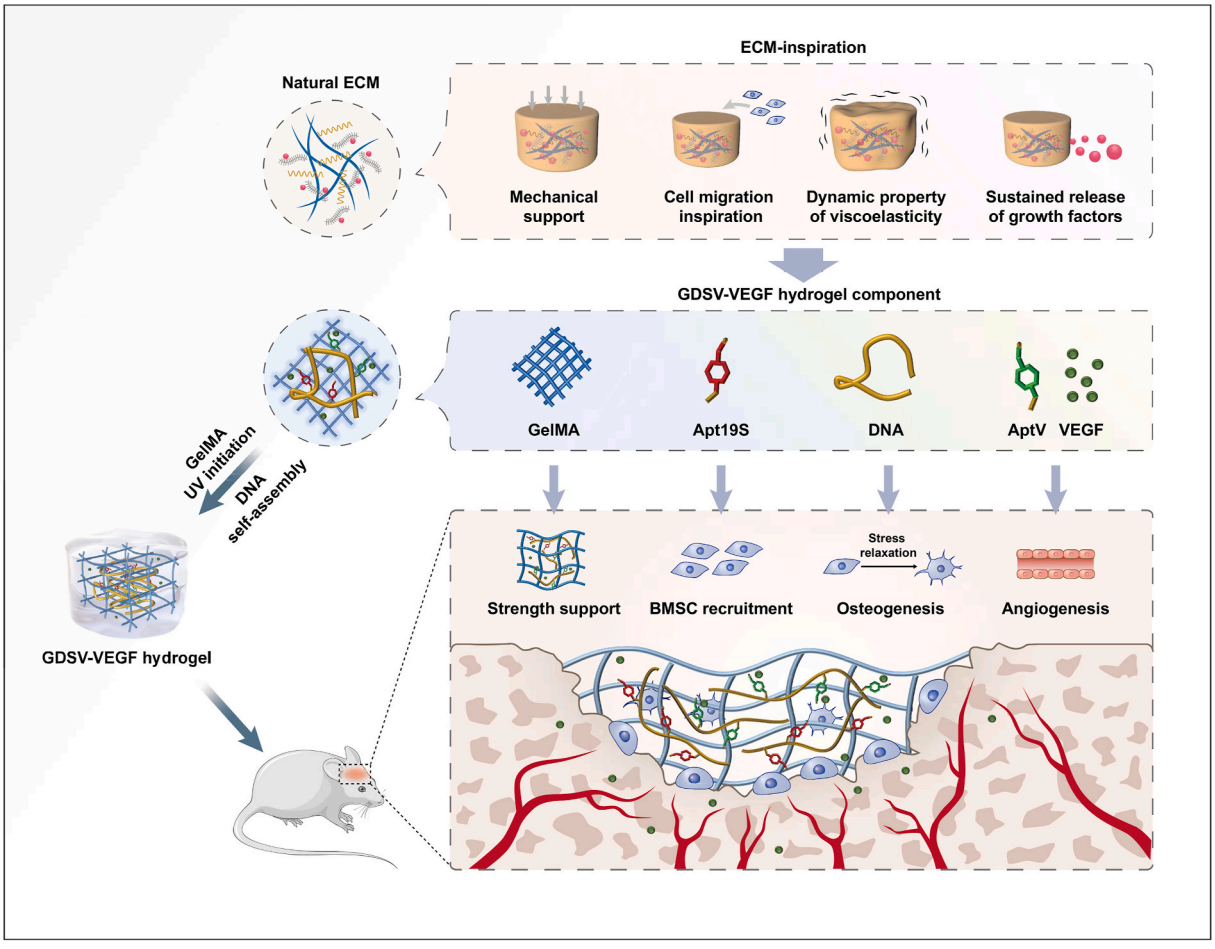

Scheme 1. Schematic of the design of the GDSV-VEGF hydrogel with ECM characteristics to promote vascularized bone regeneration.

synergistic physiological characteristics of natural bone formation (Scheme 1). The rich hydrogen bonds formed by the DNA base pairing further enhance the mechanical properties of the chemically crosslinked GelMA hydrogel, enabling it to provide mechanical support during the initial repair period to avoid collapse and unexpected degradation of the surrounding host bone structure. In addition, reversible hydrogen bond crosslinking plays a role in the viscoelasticity of double-network hydrogels to simulate the dynamic properties of the ECM. This is beneficial for hydrogel scaffolds for regulating stem cell differentiation via mechanical signal transduction. Furthermore, using Apt19S and the VEGF aptamer (AptV), the composite hydrogel is equipped with the function of recruiting BMSCs as a cell-free scaffold and providing a VEGF sustained-release platform for angiogenesis (GelMA/DNA/Apt19S/AptV, denoted as GDSV). Mechanical and structural characterizations are performed to probe the physical properties of the GDSV hydrogel. We evaluated the performance of the GDSV hydrogel in recruiting BMSCs and modulating VEGF release (GelMA/DNA/Apt19S/AptV-VEGF, denoted as GDSV-VEGF). Moreover, we evaluated the biological behaviors of the BMSCs seeded on the GDSV hydrogel including cell adhesion, proliferation and osteogenic differentiation, and detected the potential mechanism by which the GDSV hydrogel promotes osteogenesis. Furthermore, the GDSV-VEGF hydrogel was implanted into a critical-sized rat cranial bone defect model to explore the effects of vascularization-coupled bone regeneration. We expect that the composite hydrogel with functionalized DNA backbones will open new avenues for biomaterials to promote vascularized bone regeneration.

2. Materials and methods

2.1. Preparation of hydrogels

Based on the previous study [41], we aim to adapt the DNA gel by integrating aptamers. All the DNA main strands and aptamers were synthesized and verified by Sangon Biotech (Sangon, Shanghai, China). Firstly, we separately modified the two aptamers with handles. This enabled us to form the hybridized DNA main strands with the respective aptamers: TS1-Apt19S and TS2-AptV. By mixing the main strand (TS1-h1, 15785.38 g/mol) and aptamer (Apt19S-h1, 19960.98 g/mol) in phosphate buffer solution (PBS), and using concentration ratio of 100:1, we obtained the base pairing between the handles in TS1-h1 and Apt19S-h1 which resulted in the formation of TS1-Apt19S. Similarly, we formed TS2-AptV by mixing the main strand (TS2-h2, 15520.12 g/mol) with the aptamer (AptV-h2, 12716.27 g/mol), following the same method. All DNA components were characterized using a 10 % native polyacrylamide gel electrophoresis (PAGE) experiment. The DNA/Apt19S/AptV (denoted as DSV) hydrogel was assembled by the hybridization of TS1-Apt19S and TS2-AptV at a ratio of 1:1 within 1–2 min.

The GDSV hydrogel was synthesized using TS1-Apt19S, TS2-AptV, and GelMA. GelMA was synthesized by gelatin (type A, Sigma-Aldrich, USA) and methacrylic anhydride (Heowns Biochemical Technology Company, China) according to a previously described method [42]. Briefly, aqueous TS1-Apt19S and TS2-AptV were added to a GelMA solution (10%w/v) containing lithium phenyl-2,4,6-trimethylbenzoylphosphinate (LAP, Sigma-Aldrich, USA), in a volume ratio of the components was 1:1:2. Subsequently, the pre-gel was photo-polymerized under UV light (405 nm) for 1 min to realize the covalent crosslinking of GelMA, and the DNA network was simultaneously assembled within the hydrogel. The final concentrations of DNA with aptamers and GelMA were 1.5 % and 5 %, respectively. Composite hydrogels with single type of aptamer decorated DNA were also fabricated, and termed GelMA/DNA/Apt19S (GDS) and GelMA/DNA/AptV (GDV). To obtain growth factor loaded hydrogels, VEGF (# BT-VEGF-050, R&D, USA) was added into pre-gel before polymerized and the final concentration of VEGF in hydrogel was 1 μg/ml; GDSV-VEGF, GelMA/DNA/AptV-VEGF (denoted as GDV-VEGF), GelMA/DNA/Apt19S-VEGF (denoted as GDS-VEGF) and GelMA-VEGF hydrogels were fabricated. The pure GelMA hydrogel (5 % w/v) without DNA was used as a control group.

2.2. Characterization of hydrogels

2.2.1. Fluorescence images of aptamers decorated in the hydrogel

Fluorescent groups were utilized to detect whether two types of aptamers were modified in the composite hydrogel. Briefly, Alexa Fluor 350 and Cy5 (Sangon, Shanghai, China) were covalently attached to Apt19S and AptV, respectively. Then, the GDSV hydrogel was fabricated using GelMA, TS1-Apt19S-Alexa Fluor 350, and TS2-AptV-Cy5. In addition, GDS and GDV hydrogels with a single type of fluorescence group labelled aptamer were also fabricated. All the samples were observed under a fluorescence microscope (Olympus, Japan).

2.2.2. Morphology

The morphology of the obtained hydrogels was observed using a scanning electron microscopy (SEM; HITACHI, Japan) at an operating voltage of 5–10 kV, and the porosity, average pore size and distribution range of the pore sizes were analyzed by ImageJ (National Institutes of Health, USA).

2.2.3. Flourier transform infrared spectroscopy

Different groups of freeze-dried hydrogels were analyzed using a Fourier transform infrared (FTIR) spectrometer (FTIR Nicolet iN10, Thermo Scientific, USA). The spectra were acquired by averaging 64 scans with a resolution of 8 cm^{-1} in the wavenumber range of 4000-675 cm^{-1}.

2.2.4. Characterization of rheology and stress relaxation

Dynamic rheological experiments were conducted using a rheometer (Anton Paar, Austria) equipped with a 35 mm diameter plate. Frequency sweep tests were performed with frequencies ranging from 0.1 to 10 Hz under 1 % strain. The stress relaxation of different hydrogels was detected using the rheometer at a constant strain rate of 10 % for 400s.

2.2.5. Elastic modulus

The mechanical properties of the hydrogels were measured using an electromechanical tester (ZwickRoell, Germany). For compression tests of the hydrogels, the samples were cut into cylinders (4 mm in diameter and 5 mm in height) and the crosshead speed was set at 2 mm/min. The moduli of the hydrogels were obtained from the initial linear slope of the stress-strain curve.

2.2.6. Swelling ratio

Different groups of hydrogels were fabricated at a volume of 1 mL and their initial weights were recorded (W_0). All samples were then immersed in PBS at 37 °C, and the weights at different time points after immersion were recorded (W_t). The swelling ratios of the hydrogels were calculated using the following formula:

$$Swelling\ ratio = \frac{W_t - W_0}{W_0} \times 100\%$$

2.2.7. Hydrogel degradation

Different groups of hydrogels were fabricated at a volume of 1 mL and lyophilized, and their initial weights were recorded (W_0). All samples were then immersed in 1 mL PBS solution with collagenase II (1 U/mL, Sigma-Aldrich, USA) at 37 °C. At each time point, the remaining hydrogel samples were washed with ultrapure water and lyophilized, and their weights at different time points were then recorded (W_t). The mass remaining ratio of the hydrogels was calculated by the following formula:

$$Mass\ remaining\ ratio = \frac{W_t}{W_0} \times 100\%$$

2.2.8. Stability in serum-supplemented medium

By covalently attaching fluorescein amidite (FAM) groups (Sangon, Shanghai, China) to the DNA main strands, both DSV and GDSV hydrogels could exhibit green fluorescence. All samples were immersed in α-MEM (HyClone, USA) supplemented with 10 % fetal bovine serum (FBS; GIBCO, USA) and cultured at 37 °C, under 5 % CO_2. At every set time point, the medium was removed and the samples were washed three times with PBS. The samples were then observed under a fluorescence microscope, and degradation was evaluated based on the remaining fluorescent area of the hydrogels.

2.2.9. In vivo degradation of hydrogels

Twenty male 4-week-old Sprague-Dawley (SD) rats were obtained from the Renji Hospital Animal Center (Shanghai, China) to evaluate the biodegradation of hydrogels. Briefly, all groups of hydrogels were prepared into cylinders (10 mm in diameter and 3 mm in height), and their initial weights were recorded (W_0) after lyophilized. Then, hydrogels were implanted into the subcutaneous space on the back of rats. Each rat was randomly implanted two pieces of hydrogels on both sides of the spinal middle line on the back. After 14 and 28 days, the remaining hydrogels under the skin were photographed and harvested, and their remaining weights were recorded (W_t) after lyophilized. The mass remaining ratio of the hydrogels was calculated by the following formula:

$$Mass\ remaining\ ratio = \frac{W_t}{W_0} \times 100\%$$

2.3. In vitro cell activity

2.3.1. Cell culture

Male 4-week-old SD rats were used to obtain BMSCs, and cells were isolated and cultured as previously reported. Briefly, the femurs were isolated under a sterile condition, and the bone marrow was flushed out and cultured in α-MEM supplemented with 10 % FBS and 1 % penicillin/streptomycin (GIBCO, USA). After 4 days of culture, nonadherent cells were removed and fresh media were added. The remaining adherent cells were BMSCs and were passaged when they reached 80–90 % confluence. BMSCs from passages 2–4 were utilized for the subsequent *in vitro* experiments. Human umbilical vein endothelial cells (HUVECs; AllCells, China) were cultured in an endothelial cell medium (ScienCell, USA) for experiments on *in vitro* angiogenesis.

2.3.2. Live/dead staining

Live/dead staining was used to assess cell viability on different hydrogels. Briefly, in 48-well plates, 2×10^4 cells were seeded on different groups of hydrogels and the group of cells seeded directly in plate well was treated as a control. After 3 days of culture, a live/dead viability/cytotoxicity assay kit (Beyotime, China) was performed according to the manufacturer's protocol. The staining solution was added to each well and incubated for 30 min. A fluorescence microscope was used to observe the stained cells.

2.3.3. Cell counting kit-8 assay

A cell counting kit-8 (CCK-8) cell metabolism assay (Beyotime, China) was used to estimate the BMSCs proliferation activity on the different hydrogels. Briefly, in 48-well plates, 2×10^4 cells were seeded on different groups of hydrogels and the group of cells seeded directly in plate well was used as a control. After 1, 4 and 7 days of culture, the CCK-8 working solution was added to each targeted well and incubated at 37 °C, under 5 % CO_2 for 3 h. The absorbance of soluble formazan was measured at 450 nm by a microplate reader (BioTek, Winooski, VT, USA). The optical density (OD) values of the experimental, control and background groups were recorded as OD_E, OD_C and OD_B, respectively. Cell viability (%) was calculated via the following formula:

$$Cell\ viability\ (\%) = \frac{OD_E - OD_B}{OD_C - OD_B}$$

2.3.4. BMSCs homing assay

The transwell migration test (Corning Costar, USA) was used to evaluate the BMSCs homing ability of the different hydrogels. In short, 1×10^5 cells cultured in α-MEM supplemented with 10 % FBS and 1 % penicillin/streptomycin were seeded in the upper inserts with 8 μm apertures, and different hydrogels in the same medium were inoculated at the lower chambers. After 24h of co-culture, the upper cells had migrated, and the cells beneath the inserts were stained with crystal violet. The stained cells were observed under a light microscope (Olympus, Japan) and the number of migrated cells was counted.

2.3.5. The release kinetics of VEGF from hydrogels

Different groups of hydrogels (volume: 1 mL) loaded with VEGF at a concentration of 1 μg/ml were placed in sterile Eppendorf tubes, and 2 mL of endothelial cell medium was added. The GDSV hydrogel without VEGF was added to the same solution as the control group for the tube formation assay. At every set time point, the medium was extracted and fresh endothelial cell medium was supplemented. The released VEGF was quantitatively analyzed via Human VEGF ELISA kit (R&D, USA). The cumulative release percentage of VEGF was calculated according to the released VEGF divided by the total amount of VEGF loaded into the hydrogels.

2.3.6. Tube formation assay

Growth factor reduced Matrigel (Corning, USA) was added into 48-well plates on ice and incubated at 37 °C for 30 min to realize gelation. HUVECs were collected and resuspended in different extracted media obtained from the release VEGF assay (1, 6, 10 days). Then, HUVECs were seeded onto the Matrigel at 1×10^5 cells/well. After incubation at 37 °C, under 5 % CO_2 for 3 h, the tube formation was observed under a light microscope and the total tube lengths, nodes and meshes were calculated using ImageJ software.

2.3.7. Alkaline phosphatase activity

In order to detect the alkaline phosphatase (ALP) activity, BMSCs were seeded on different hydrogels in an osteogenic differentiation medium (Cyagen Biosciences, USA). After 7 days of culture, all groups were fixed with 4 % paraformaldehyde for 10 min and washed three times with PBS. An ALP staining kit (Beyotime, China) was used to stain the cells according to the manufacturer's protocol. For the ALP quantification assay, all samples were treated with p-nitrophenyl phosphate (p-NPP) (Sigma-Aldrich, USA) at 37 °C for 30 min. ALP activity was measured using a microplate reader at 405 nm, and the obtained OD values were normalized to the total protein concentration of each group detected using a protein assay kit (Thermo Fisher Scientific, USA).

2.3.8. Calcium deposition assay

For the calcium deposition assay, all groups were stained with alizarin red S (ARS) solution after 14 days of culture. After observation under a light microscope, the stained samples were desorbed by 10 % cetylpyridinium chloride (Sigma-Aldrich, USA) and the OD values were measured at 562 nm. The quantification of calcium deposition was also normalized to the total protein.

2.3.9. Quantitative real-time polymerase chain reaction

The expression of osteogenesis-related genes was evaluated by a quantitative real-time polymerase chain reaction (qPCR). Briefly, BMSCs were cultured on different hydrogels in an osteogenic differentiation medium, and the total RNA was extracted using Trizol reagent (Invitrogen, USA) after 7 days. The total RNA was reverse-transcribed to

cDNA via a PrimeScriptfirst strand cDNA synthesis kit (Takara, Japan), and the cDNA was mixed with SYBR Green Master Mix (Roche, Switzerland). The gene expressions of RUNX family transcription factor 2 (*Runx2*), Sp7 transcription factor (*Osterix*), collagen type 1 (*Col1*), *Alp*, and osteocalcin (*Ocn*) were measured by a PCR system (LightCycler LC480, Roche, Switzerland). All genes were normalized to the housekeeping gene *β-actin*, and the GelMA group was used as a control. The primer sequences are listed in Table 1.

2.4. In vivo angiogenesis and osteogenesis assays

2.4.1. Surgical procedure

Male 8-week-old SD rats were used to establish a cranial bone defect model according to previously reported protocols. The animal procedures were reviewed and approved by the Institutional Animal Care and Use Committee of Renji Hospital, Shanghai Jiao Tong University School of Medicine. In order to evaluate the osteogenesis of the hydrogels, 15 SD rats were anesthetized and two critical-sized defects (diameter of 5.0 mm) were created on the calvarium of each rat using an electric trephine. The different hydrogels were randomly implanted in the 30 critical-sized defects and divided into five groups: blank control group (n = 6), GelMA group (n = 6), GelMA-VEGF group (n = 6), GDSV group (n = 6) and GDSV-VEGF group (n = 6). Meanwhile, another 15 SD rats were subjected to the same surgical procedure to evaluate the angiogenesis of the hydrogels.

2.4.2. Sequential fluorescent labeling

Polychrome sequential fluorescent labeling was applied for evaluating dynamic bone mineralization as previously reported [43]. Four and six weeks after the operation, the 15 rats used for evaluation of osteogenesis were administered an intraperitoneal injection with ARS (30 mg/kg, Sigma-Aldrich, USA) and calcein (CA; 20 mg/kg, Sigma-Aldrich, USA), respectively.

2.4.3. Micro-CT analysis of new bone formation

Eight weeks after the operation, the 15 rats used for the evaluation of osteogenesis were euthanized by overdose of anesthesia. The calvariums were collected and fixed in 4 % paraformaldehyde. Referring to a previous method, all samples were scanned by a micro-CT machine (μCT 80, Scanco Medical, Switzerland) at an isometric resolution of 18 μm and the morphology of the calvariums was reconstructed. The bone volume/total volume (BV/TV) ratio and bone mineral density (BMD) in the region of interest (ROI) were analyzed using an accompanying software.

2.4.4. Histological analysis of new bone formation

After micro-CT analysis, all specimens were dehydrated and embedded in polymethylmethacrylate (PMMA). The embedded specimens were cut into 150 μm undecalcified sections by a microtome (SP1600, Leica, Germany), and then polished to a final thickness of approximately 40 μm. Confocal laser scanning microscopy (CLSM; Olympus, Janpan) was applied to detect the polychromefluorescent labeling. The excitation/emission wavelengths of 543/600−640 nm and 488/500−550 nm were chosen to observe ARS (red) and CA (green), respectively. The percentages of the fluorescent area were quantified by ImageJ. After detecting the polychromefluorescent labeling, all sections were stained with Van Gieson's (VG) picrofuchsin to observe new bone tissue. In addition, other polished sections were put into ethylene glycol ethyl ether acetate to remove the embedding agent. After rehydration, all sections were stained with Masson's trichrome for the observation of new bone formation. A microscope was used to capture images and the percentages of new bone formation were quantified by ImageJ software.

Table 1
List of primer sequences used for qPCR.

Species	Gene	Primer	Sequence (5'→3')
Rat	*Runx2*	F	CTTCGTCAGCGTCCTATCAGTTCC
		R	TCCATCAGCGTCAACACCATCATTC
Rat	*Osterix*	F	CTTGGATATGTCCCATCCCTAC
		R	CAAAGTCAGACGGGTAAGTAGG
Rat	*Col1*	F	GGATCGACCCTAACCAAGGC
		R	GATCGGAACCTTCGCTTCCA
Rat	*Alp*	F	CACGGCGTCCATGAGCAGAAC
		R	CAGGCACAGTGGTCAAGGTTGG
Rat	*Ocn*	F	CTGAGTCTGACAAAGCCTTCAT
		R	TCCAAGTCCATTGTTGAGGTAG
Rat	*β-actin*	F	TTCGCCATGGATGACGATATC
		R	TAGGAGTCCTTCTGACCCATAC

2.4.5. Microfil perfusion and micro-CT analysis of new blood vessels

The 15 rats used for the evaluation of angiogenesis were administered a microfil perfusion 8 weeks after the operation. Briefly, after anesthesia, the thorax of each rat was exposed. The descending aorta was ligated, and a catheter was inserted from the left ventricle to the aorta. Subsequently, heparinized saline was perfused to remove blood and Microfil (MV-120, Flow Tech, USA) was perfused from the left ventricle to the circulatory system. Then, all rats were placed under refrigeration at 4 °C overnight to ensure polymerization. The calvariums were harvested, fixed and decalcified in 10 % EDTA. A micro-CT scan of the decalcified calvariums was obtained with a voltage of 40 kV, an electric current of 250 mA and an exposure time of 240 ms. Scanning was performed at an isotropic resolution of 9 μm, and the new blood vessels formed in bone defects were analyzed by the accompanying CTVol software.

2.4.6. Immunofluorescence assay of CD31

After the micro-CT analysis for new blood vessels, all decalcified samples were embedded in paraffin and cut into 4 μm thickness sections. Paraffin sections were co-incubated with a primary antibody of anti-CD31 (ab222783, Abcam, UK; 1:100), and then incubated with a DyLight594 (ab96885, Abcam, UK; 1:200) as the corresponding secondary antibody. The sections were then counterstained with DAPI (Sigma-Aldrich, USA) and observed under CLSM. The percentages of positively stained CD31 areas were analyzed by ImageJ.

2.5. Detecting the mechanism and role of osteogenic differentiation

2.5.1. RNA sequencing

BMSCs on different hydrogels were collected, and the total RNA was extracted using Trizol reagent and purified using a NEBNext Poly (A) mRNA Magnetic Isolation Module Kit (E7490, NEB, USA). Library sequencing was performed using an Illumina NovaSeq 6000 instrument according to the manufacturer's instructions. Gene Ontology (GO) and Kyoto Encyclopedia of Genes and Genomes (KEGG) pathway enrichment analyses were performed based on the differentially expressed genes (DEGs) obtained from RNA sequencing (RNA-seq).

2.5.2. Immunofluorescence assay of cytoskeleton

After the BMSCs were seeded on the different hydrogels for 24 h, the samples were fixed in 4 % paraformaldehyde for 20 min and permeabilized in 0.1%Triton X-100 for 10 min. After blocking with 3 % bovine serum albumin (BSA, Sigma-Aldrich, USA) for 30 min, the samples were incubated with Phalloidin-iFluor 488 (Abcam, UK) for 1 h to the stain cytoskeleton (F-actin) and counterstain with DAPI for another 10 min. All specimens were observed under CLSM and the spread areas of F-actin were analyzed by ImageJ.

2.5.3. Western blot analysis

The protein level of the molecular mechanism was analyzed by Western blot. Briefly, the total cell protein was collected using a protein extraction regent (Beyotime, China) and the concentration was determined using a protein assay kit. Equal amounts of protein samples were separated in sodium dodecyl sulfate and PAGE, and then transferred to polyvinylidene fluoride membranes (PVDF, Millipore, USA). After

blocking in 5 % BSA for 1 h, membranes were incubated with primary antibodies in 5 % BSA at 4 °C overnight. The membranes were then incubated with the corresponding secondary antibody (ab205718, Abcam, 1:20000) at room temperature for 1 h. The membranes were visualized using a molecular imaging system (Bio-Rad, USA) and the protein gray values were quantified by ImageJ. The primary antibodies of focal adhesion kinase (FAK, ab40794, Abcam, UK; 1:2000), phosphor-FAK (p-FAK, ab81298, Abcam, UK; 1:1000), protein kinase B (Akt,

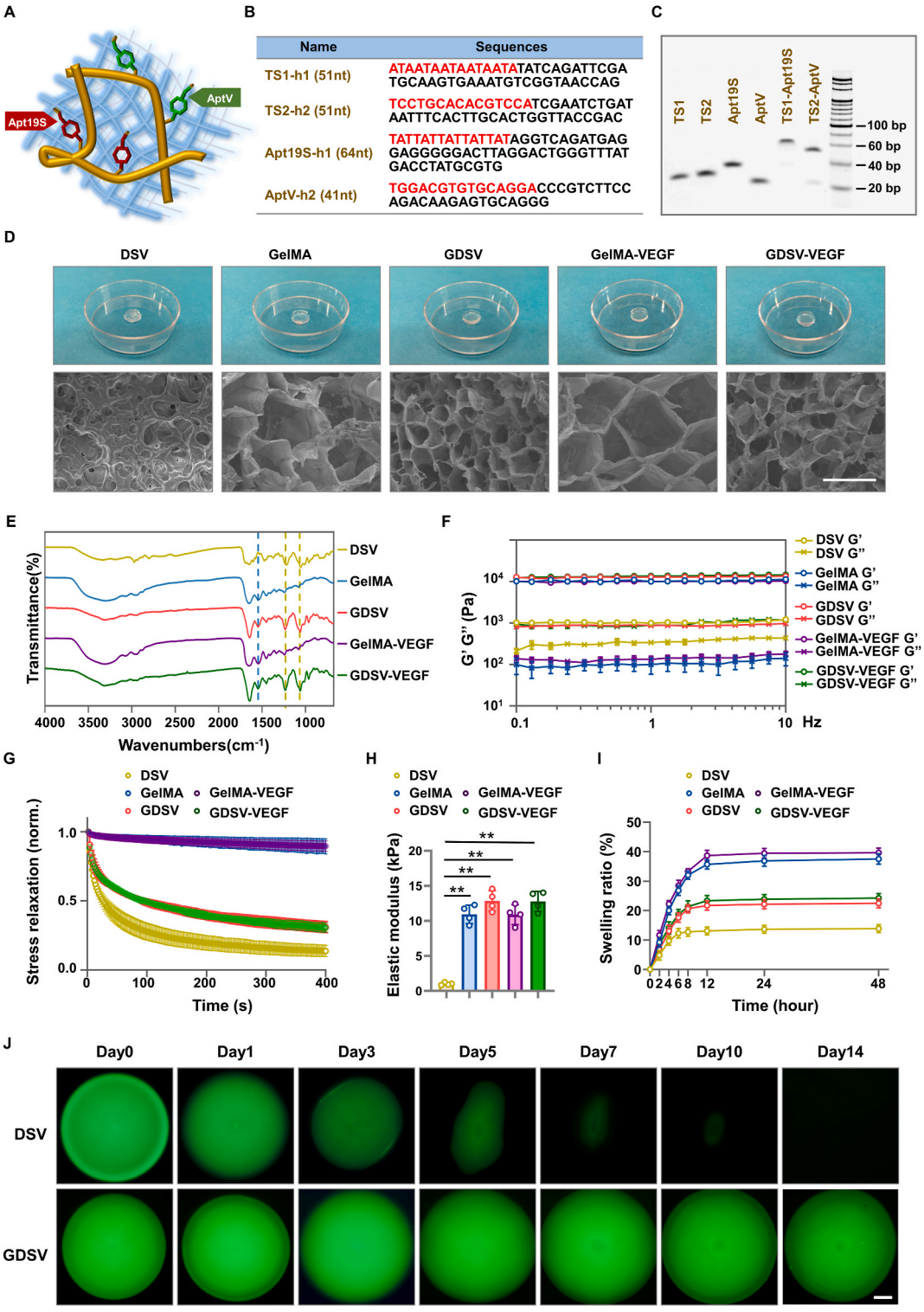

Fig. 1. Synthesis and characterization of GDSV hydrogel. A) Schematic of the structure of GDSV hydrogel. B) Sequence information of DNA components ("handles" sequences are labelled as red letters). C) Native PAGE of DNA components. D) Macroscopic appearance and SEM images of the DSV, GelMA, GDSV, GelMA-VEGF, and GDSV-VEGF hydrogels, scale bar = 100 μm. E) FTIR spectra of the DSV, GelMA, GDSV, GelMA-VEGF, and GDSV-VEGF hydrogels. F) Storage modulus (G′) and loss modulus (G″) of hydrogels (n = 4). G) Normalized stress relaxation of the DSV, GelMA, GDSV, GelMA-VEGF, and GDSV-VEGF hydrogels (n = 4). H) Elastic modulus of hydrogels (n = 4, $^{**}p < 0.01$). I) Swelling profile of the DSV, GelMA, GDSV, GelMA-VEGF, and GDSV-VEGF hydrogels (n = 4). J) Fluorescence images showing FAM labelled DSV and GDSV hydrogels via observation of remaining fluorescent area in serum-supplemented medium, scale bar = 500 μm.

ab179463, Abcam, UK; 1:10000), phosphor-Akt (p-Akt, ab81283, Abcam, UK; 1:8000), β-Catenin (ab32572, Abcam, UK; 1:8000), Runx2 (ab236639, Abcam, UK; 1:1000) and GAPDH (ab181602, Abcam, UK; 1:10000) were utilized, and these protein expression were tested in this assay.

2.6. Statistical analysis

All the data were presented as the mean ± standard deviation (SD). Statistical analyses were performed using a Student's t-test or one-way ANOVA, followed by a post hoc test for multiple comparisons using GraphPad software (GraphPad Software, Inc., USA). Statistical differences were considered to be significant when $p < 0.05$ or $p < 0.01$.

3. Results and discussion

3.1. Synthesis and characterization of GDSV hydrogel

In this study, we fabricated a composite hydrogel comprising a double network of GelMA and DNA decorated with aptamers to the treat bone defects (Fig. 1A). The sequence design of the DNA structure was listed and the composition of the DNA was confirmed (Fig. 1B and C). The fluorescence images shown in Fig. S1 demonstrated that two types of aptamers were successfully modified in the GDSV hydrogel, as it exhibited blue and red fluorescence simultaneously. As shown in Fig. 1D, the DSV, GelMA, GDSV, GelMA-VEGF, and GDSV-VEGF hydrogels were fabricated; and the SEM images revealed the microporous structures of the hydrogels. The DNA network of DSV was denser and had a smaller pore size than GelMA, indicating that GelMA and DSV could form hydrogels with different micro morphologies through covalent and physical crosslinking, respectively. The GDSV hydrogel exhibited combined characteristics with a clear network structure similar to that of GelMA and pore size similar to that of DSV. In addition, the micro morphologies of GelMA-VEGF and GDSV-VEGF hydrogels were similar to that of GelMA and GDSV hydrogels, respectively. The pore size and porosity of DSV, GelMA, GDSV, GelMA-VEGF, and GDSV-VEGF hydrogels were 71.2 ± 10.88 μm and 46.12 ± 3.58 %, 100.21 ± 11 μm and 60.03 ± 4.85 %, 67.78 ± 7.1 μm and 53.28 ± 3.74 %, 102.3 ± 6.88 μm and 61.31 ± 5.54 %, and 69.06 ± 7.75 μm and 54.79 ± 4.19 %, respectively (Fig. S2A). In addition, we analyzed the distribution range of pore sizes. As shown in Fig. S2B, compared with the DSV group, the pore sizes of GDSV and GDSV-VEGF were uniform and the majority of diameters were approximately in the range of 65–70 μm, and the pore sizes of GelMA and GelMA-VEGF were mostly in the range of 100–110 μm. Similar to the double network hydrogel showing the composite morphology of polyacrylamide (PAM) and DNA under the microscopic scale [44], the SEM result indicated that the interpenetrating networks of GelMA and DNA was formed in the GDSV hydrogel. The characteristic peaks of the hydrogels were determined using FTIR. As shown in Fig. 1E, the GelMA, GelMA-VEGF, GDSV, and GDSV-VEGF hydrogels showed the characteristic amino peaks (N-H bending, amide II) of gelatin at approximately 1540 cm^{-1} [45,46]. In contrast to GelMA, DSV showed the characteristic DNA peaks of PO_2^- asymmetric stretching (1219 cm^{-1}) and ribose C-C stretching (1054 cm^{-1}) [39], which were also observed in the spectra of GDSV and GDSV-VEGF at approximately 1233 and 1059 cm^{-1}.

Excellent mechanical properties enable hydrogels to provide both physical support during the initial stages of repair and physiological cues to induce bone formation. The mechanical properties of each hydrogel were examined via a series of tests. Based on the results of the frequency sweep test (Fig. 1F), all groups exhibited a plateau appearing of the storage modulus (G′), which was significantly higher than the loss modulus (G″). These results suggested that all groups showed the typical mechanical properties of hydrogel with a relatively complete network structure. Interestingly, the G''/G′ ratios (Loss factor, tanδ) were approximately 33 %, 1 %, and 7 % in DSV, GelMA, and GDSV, respectively. In addition, loading VEGF did not affect the tanδ of hydrogels, and the ratios of GelMA-VEGF and GDSV-VEGF were still approximately 1 % and 7 %, respectively. According to previous reports, the ratio in natural tissues is approximately 10 %, indicating that the GDSV hydrogel possessed similar properties of tanδ to those of natural tissues [8,23]. The mechanical environment of natural bone ECM is dynamic and exhibits rapid stress relaxation characteristics, which plays an essential role in adjusting the biological behavior of cells [8,9]. Previous studies have reported that hematoma formation in bone defects exhibits rapid stress relaxation, which is necessary for bone healing [6,10,47]. Physically-crosslinked alginate hydrogels with rapid stress relaxation can mimic hematomas and promote new bone formation, even without encapsulating seed cells or growth factors [48]. The GDSV and GDSV-VEGF hydrogels displayed typical rapid stress relaxation behavior, which was considerably different from that of the elastic GelMA and GelMA-VEGF hydrogels (Fig. 1G). Recent developments in dynamic chemistry have revealed that adaptable hydrogels with rapid stress relaxation can be obtained from many non-covalent interactions, including electrostatic interactions, hydrophobic interactions, macrocyclic host-guest interactions and hydrogen bonds [49,50]. Theoretically, as a substance rich in hydrogen bonds, DNA is ideal for the fabrication of adaptable hydrogels [51]. However, whether DNA based hydrogels can perform desirable rapid stress relaxation, which is beneficial for promoting bone formation, remains unclear. Our results suggest that the rapid stress relaxation behavior of GDSV can be attributed to the physical crosslinking of the DNA network. In addition, the DSV hydrogel completed the stress relaxation process in a shorter time than GDSV. The stress relaxation times ($T_{1/2}$) were approximately 29s and 100s for DSV and GDSV, respectively. Similar to that of GDSV, the $T_{1/2}$ was approximately 98s for GDSV-VEGF. It is known that the degree of relaxation of a hydrogel is closely related to its mode of crosslinking. For the GDSV hydrogel, the DNA network with physical crosslinking helped accelerate stress relaxation, whereas the GelMA network with covalent crosslinking limited relaxation to some extent. Interestingly, previous studies have reported that the stress relaxation time of fracture hematoma and ECM-like hydrogels which could promote osteogenesis was about 60–200s [6,48]. The timescale of the stress relaxation of the GDSV hydrogel appeared to approach that of the natural fracture hematomas and other ECM-like hydrogels which could promote osteogenesis. When detecting the mechanical strength of hydrogels (Fig. 1H), GelMA (10.94 ± 1.32 kPa) and GDSV (12.86 ± 1.46 kPa) hydrogel displayed similar elastic moduli with no statistically significant difference, which were considerably higher than that of DSV (1.01 ± 0.17 kPa). In addition, the GelMA-VEGF (10.9 ± 1.41 kPa) and GDSV-VEGF (12.77 ± 1.43 kPa) displayed similar elastic moduli to that of GelMA and GDSV, respectively. This result indicated that the pure DNA hydrogel was relatively soft and lacked sufficient mechanical strength as a scaffold for bone repair.

It has been proven that the double network strategies can not only improve the mechanical performance of hydrogels, but also regulate the swelling and degradation properties [52,53]. Hence, the swelling property was also detected, as shown in Fig. 1I, where the GelMA, GelMA-VEGF, GDSV, and GDSV-VEGF hydrogels reached the equilibrium swelling state after immersion in PBS for approximately 12 h, and DSV reached the equilibrium state after approximately 8 h. The swelling ratios at 48 h were 13.86 ± 1.35 %, 37.53 ± 1.79 %, 39.66 ± 1.61 %, 22.48 ± 1.52 %, and 24.23 ± 1.56 % in DSV, GelMA, GelMA-VEGF, GDSV, and GDSV-VEGF, respectively. In order to evaluate the degradation behavior of the hydrogels, the DSV, GelMA, GelMA-VEGF, GDSV, and GDSV-VEGF hydrogels were cultured in a collagenase II solution. As shown in Fig. S3, both the GelMA and GelMA-VEGF hydrogels were completely degraded after 24 h, whereas the degradation of the GDSV and GDSV-VEGF hydrogels were retarded, and the hydrogels remained in the solution for a longer period. The retarded degradation performance of the GDSV and GDSV-VEGF hydrogels was attributed to the more compact structure of the double network and insensitivity of the

DNA macromolecules to collagenase II. In contrast to GelMA, pure DNA hydrogels are susceptible to unintentional degradation in a serum-supplemented medium owing to the common inclusion of deoxyribonuclease I [51]. Hence, the stability of the hydrogels with the DNA network was tested in α-MEM supplemented with 10 % FBS. Using fluorescence group labelled DNA strands, the degradation of the DSV and GDSV hydrogels was clearly monitored under a fluorescence microscope. As shown in Fig. 1J, by observing the remaining fluorescent area of hydrogels, we found that DSV began to degrade after immersion in the serum-supplemented medium for approximately 3 days and completely degraded after 14 days. However, GDSV exhibited no perceptible degradation after 14 days of immersion from the observation of stable fluorescent area. Furthermore, after subcutaneous implantation into the back of rats, the hydrogels also exhibited different biodegradation. As is shown in Figs. S4A and B, the DSV hydrogel degraded rapidly, with 15.33 ± 5.37 % mass remain after 14 days, and was completely resorbed after 28 days. Different from the pure DNA hydrogel, GelMA hydrogels exhibited slower biodegradation performances: the mass remaining rate of GelMA and GelMA-VEGF hydrogels were 56.58 ± 4.7 % and 58.86 ± 4.98 % after 14 days, and 30.92 ± 3.53 % and 33.67 ± 4.12 % after 28 days, respectively. Compared with the single network hydrogels, the double network hydrogels exhibited the slower biodegradation performances: the mass remaining rate of GDSV and GDSV-VEGF hydrogels were 66.69 ± 4.38 % and 69.5 ± 5.68 % after 14 days, and 39.22 ± 4.62 % and 41.43 ± 3.68 % after 28 days, respectively. The results of degradation indicated that the pure DNA hydrogel was unstable in serum-containing environments *in vitro* or the physiological environment *in vivo*, and the combinations of DNA structures and polymeric compounds, such as GelMA, could improve the stability.

Taken together, these results demonstrated that, with the addition of DNA network, the GDSV and GDSV-VEGF hydrogels exhibited obvious rapid stress relaxation. Moreover, owing to the stable GelMA network, the GDSV and GDSV-VEGF hydrogels can provide suitable mechanical properties to support bone tissue regeneration and overcome the instability of pure DNA in the physiological environment. In addition, because VEGF does not participate in the crosslink of networks formed by GelMA and DNA main strands, the GelMA-VEGF and GDSV-VEGF hydrogels exhibit similar material characterizations to the GelMA and GDSV hydrogels respectively, which is consistent with the previous study about VEGF-loaded hydrogels [54].

3.2. GDSV hydrogel biocompatibility and promotion of cell proliferation

Live/dead staining was used to evaluate the cytotoxicity of the GDSV hydrogel towards BMSCs. As shown in Fig. 2A, bright green fluorescence was observed in all groups, whereas red fluorescence was extremely rare among the different hydrogels. The status of BMSCs was viable on GDSV hydrogels with or without VEGF, and had no distinguishable disparities compared with BMSCs seeded in plate wells (control group). Cell proliferation was measured using the CCK-8 assay (Fig. 2B), and a time-dependent growth trend of BMSCs was observed in all groups. The

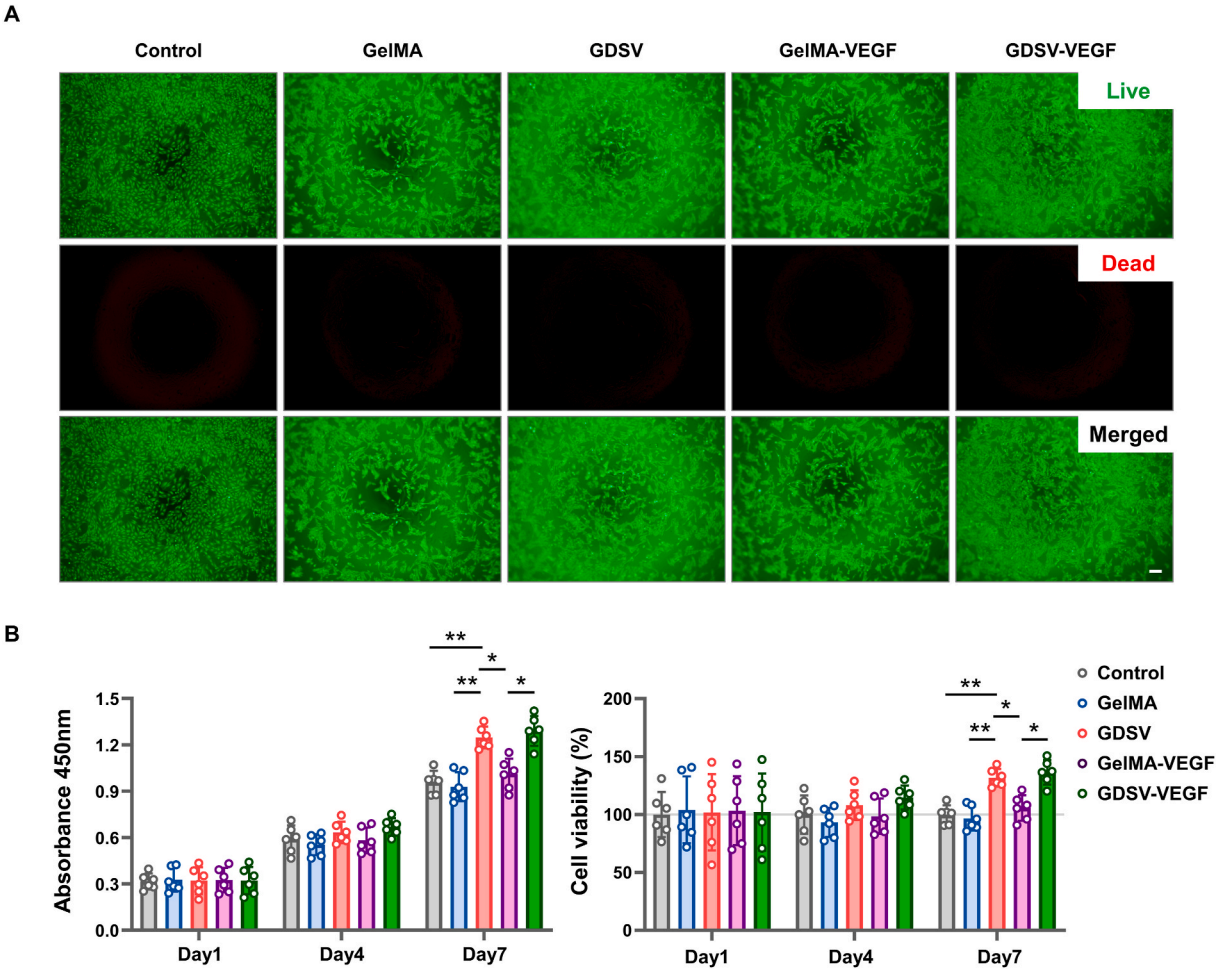

Fig. 2. GDSV hydrogel biocompatibility and promotion of cell proliferation. A) Live/dead staining of BMSCs on GelMA, GelMA-VEGF, GDSV, and GDSV-VEGF hydrogels after 3 days of culture. Viable cells are green and dead cells are red, control group: BMSCs seeded in plate well directly, scale bar = 200 μm. B) CCK-8 assay of BMSCs proliferation and viability on different hydrogels for 1, 4 and 7 days (n = 6, *$p < 0.05$, **$p < 0.01$).

proliferation activity on day 7 in the GDSV group was markedly higher than those in the GelMA, GelMA-VEGF, and control groups. Furthermore, the cell viabilities of the GDSV on day 7 were markedly elevated and significantly different from those of the GelMA group. We suppose that the facilitation of BMSCs proliferation is owing to the fast stress relaxation property of the GDSV hydrogel. Previous studies have proved substrate with fast stress relaxation can promote cell proliferation such as MSCs, fibroblasts and myoblasts [55–57]. According to our material characterization results, compared with GelMA hydrogel, the GDSV hydrogel exhibited significant matrix viscoelasticity of fast stress relaxation which was similar to ECM. In addition, although the GDSV-VEGF group showed the highest OD value and cell viability on day 7, no significant difference was observed between the GDSV-VEGF and GDSV groups, suggesting that VEGF could contribute to promoting BMSCs growth, but was not the decisive factor. Taken together, the live/dead staining and CCK-8 results implied that the GDSV hydrogel was biocompatible and capable of stimulating BMSCs proliferation.

3.3. GDSV hydrogel for promoting the homing of BMSCs

Transwell migration experiments were conducted to explore the role of the GDSV hydrogel in BMSCs recruitment (Fig. 3A and B). As shown in Fig. 3C and D, only a few cells migrated in the control, GelMA, and GDV groups. However, a marginally higher number of migrating cells was observed in the GelMA-VEGF and GDV-VEGF groups. This could be attributed to the chemotactic effects of VEGF on BMSCs [58]. Interestingly, a significant number of BMSCs was observed in the GDSV and GDSV-VEGF groups. This indicated that the inclusion of aptamer Apt19S in the hydrogels effectively recruited stem cells. The migration of endogenous stem cells to the site of injury is a crucial step in tissue regeneration. The sufficient migration of BMSCs to the defect area has a great contribution to facilitate bone formation [32,59]. Therefore, this finding suggests that the GDSV hydrogel can potentially be used as a candidate material for bone tissue repair.

3.4. GDSV-VEGF hydrogel for promoting tube formation via sustained-release of VEGF

The sustainable release of VEGF is important for maintaining its effective activity and concentration in hydrogels, which can promote angiogenesis (Fig. 4A). Fig. 4C shows the cumulative release of VEGF from GelMA-VEGF, GDS-VEGF, and GDSV-VEGF hydrogels over 14 days. Both the GelMA-VEGF and GDS-VEGF hydrogels exhibited an initial burst release of approximately 50 % of the total amount loaded within the first 2 days, followed by a gradual decrease in the release rate. In contrast, GDSV-VEGF showed a slower release rate, with only 22 % of the total loaded VEGF released within the first 2 days. This hydrogel exhibited sustainable release behavior, and the cumulative release of VEGF was approximately 70 % after 14 days. These results suggest that the GDSV-VEGF hydrogel has the potential to maintain a sustained VEGF release over time, which may be beneficial for promoting angiogenesis and facilitating tissue regeneration.

Because the tube formation assay is an effective method to evaluate angiogenetic activities (Fig. 4B), HUVECs treated with extracts from different groups at different time points were investigated, and the total tube lengths, nodes, and meshes were quantified. As shown in Fig. 4D, vascular structures were formed within the capillary nets in extracts of every time point from the GDSV-VEGF hydrogel. In contrast, vascular nets were only observed under extracts of day 1 from GelMA-VEGF and GDS-VEGF hydrogels. When treated with the extracts of day 6 and day

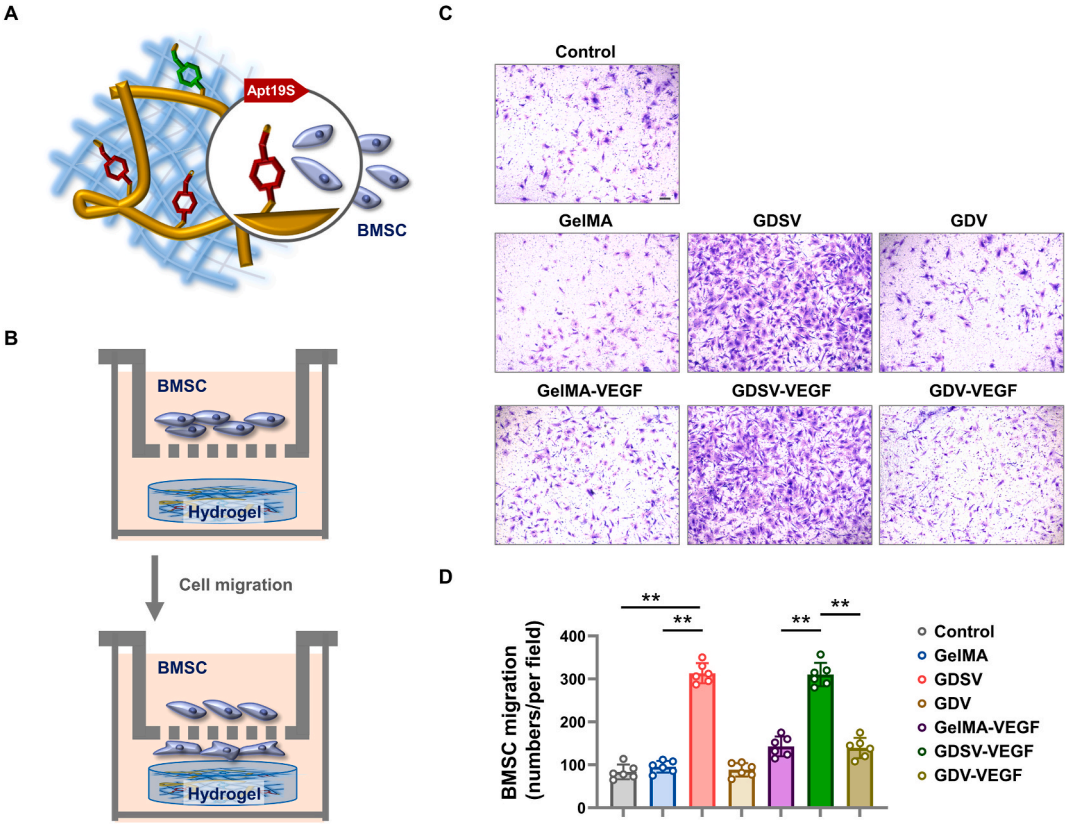

Fig. 3. GDSV hydrogel for promoting the homing of BMSCs. A) Schematic of the DNA aptamer (Apt19S), which performs the function of BMSCs recruitment. B) Illustration of the transwell migration test. C) BMSCs that traversed the membranes were stained. Images of cells towards GelMA, GelMA-VEGF, GDSV, GDSV-VEGF, GDV and GDV-VEGF hydrogels were captured, control group: no hydrogel was placed in the lower chamber, scale bar = 100 μm. D) Quantitative analysis of migrated BMSCs (n = 6, $^{**}p < 0.01$).

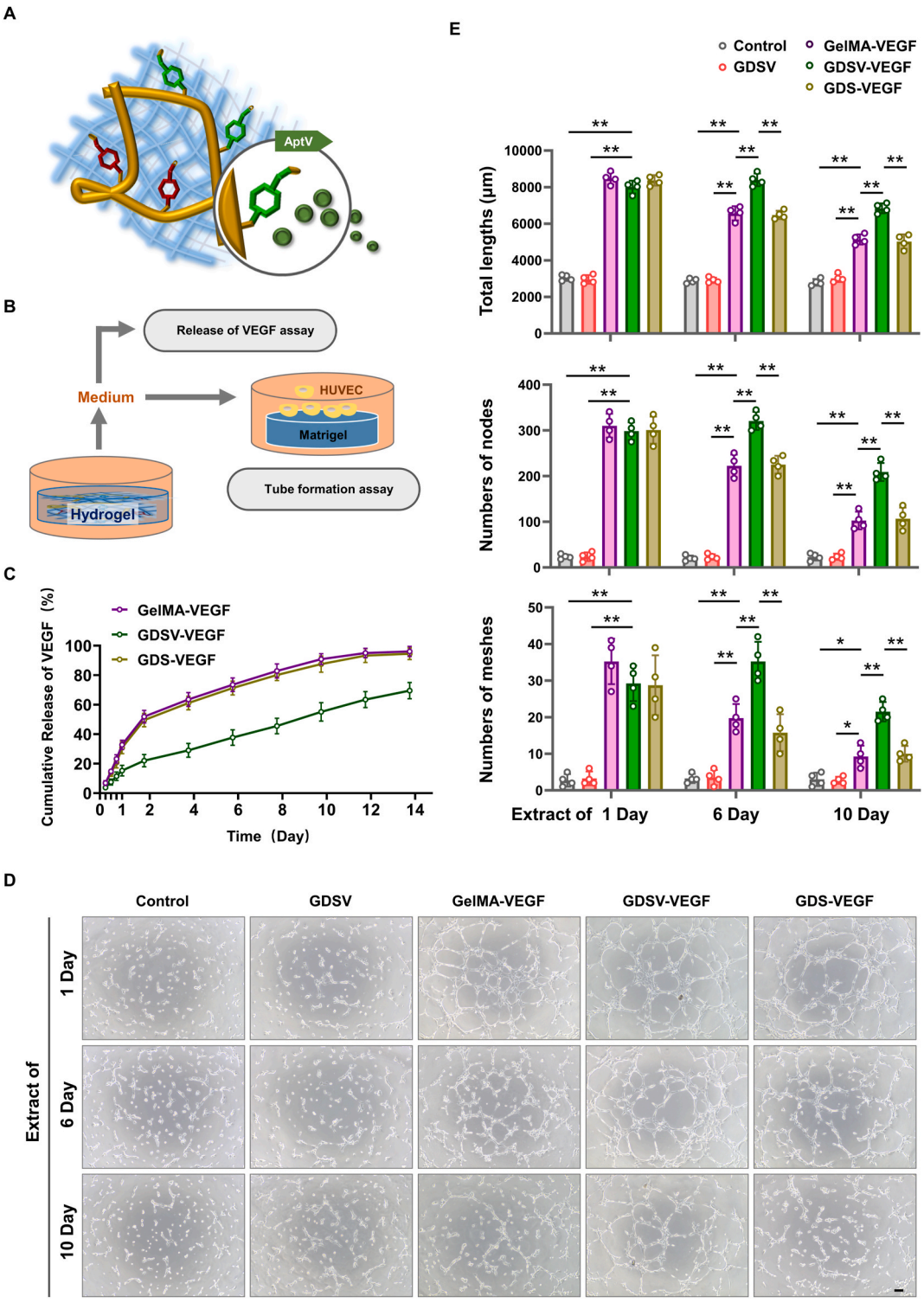

Fig. 4. GDSV-VEGF hydrogel for promoting tube formation via sustained-release of VEGF. A) Schematic of the DNA aptamer (AptV) which performs the function of the sustained-release of VEGF. B) Illustration of extract from medium with hydrogel to detect release of VEGF and tube formation. C) VEGF cumulative release curve of GelMA-VEGF, GDSV-VEGF, and GDS-VEGF hydrogels (n = 4). D) Images of tube formation of HUVECs under extracts from GDSV, GelMA-VEGF, GDSV-VEGF and GDS-VEGF hydrogels at time points of 1, 6, and 10 days, control group: extract from medium without hydrogel, scale bar = 200 μm. E) Quantitative analysis of total lengths, nodes and meshes numbers (n = 4, $*p < 0.05$, $**p < 0.01$).

10, both the GelMA-VEGF and GDS-VEGF hydrogels failed to generate obvious capillary nets. The quantitative results of the tube length, node, and mesh numbers were consistent with observations from the different groups (Fig. 4E). These results demonstrated that AptV could help prolong the function of the hydrogel as a VEGF release platform to promote angiogenesis.

In addition, the results of the transwell migration and release kinetics of VEGF tests indicated that aptamers with definite functions were successfully connected to the DNA network. Previous studies reported that aptamers could be modified on the surface of graphene or collagen

via coupled reactions [31,34]. In our study, by designing specific base sequences, namely "handles" at the ends of aptamers and main strands, aptamers could be easily combined with the DNA network. Compared with the use of chemical coupling agents, obtaining aptamer modified hydrogels via the DNA base complementation is more convenient and effective. Owing to the specific functions of Apt19S and AptV modified on the composite hydrogel, the GDSV-VEGF hydrogel exhibited the positive ability to recruit BMSCs and continuously release VEGF for long-term angiogenesis.

3.5. GDSV hydrogel for enhancing BMSCs osteogenic differentiation in vitro

The detection of ALP activity and calcium deposition was effective for evaluating the osteo-inductivity of the different hydrogels. As shown in Fig. 5A, compared with the other two groups, both the GDSV and GDSV-VEGF groups displayed higher ALP activity with a deeper staining intensity. The quantitative results of ALP showed that (Fig. 5B), the GDSV group exhibited significantly increased ALP activity compared with the GelMA and GelMA-VEGF groups, and the GDSV-VEGF group exhibited the highest ALP activity. Similar results were observed for calcium deposition via ARS staining (Fig. 5A), the number of mineralized nodules and positively stained areas of calcium deposition were significantly augmented in the GDSV and GDSV-VEGF groups (Fig. 5B). To investigate the influence of different hydrogels on the differentiation of BMSCs at the molecular level, the expressions of osteogenic-related genes including *Runx2*, *Osterix*, *Col1*, *Alp*, and *Ocn* were measured by qPCR. As shown in Fig. 5C, compared with the GelMA and GelMA-VEGF groups, the expressions of all these genes were significantly up-regulated in the GDSV group. Moreover, the GDSV-VEGF group displayed the highest elevating expressions of osteogenic-related genes, which may be due to the fact that VEGF directly triggers the osteogenic differentiation of osteoblast-related cells through its receptors [60]. However, no significant difference was observed between the GDSV and GDSV-VEGF groups, consistent with the ALP activity and calcium deposition results. Taken together, the above results proved that the GDSV hydrogel has great potential to enhance the osteogenic differentiation of BMSCs *in vitro*.

3.6. GDSV-VEGF hydrogel for promoting vascularized bone formation in vivo

The potential of the hydrogels to promote new bone formation and neovascularization was assessed using a rat cranial defect model. Micro-CT reconstruction was performed to estimate cranium regeneration in the different groups. As shown in Fig. 6A, growth of new bone from the edge of the defect towards the center was observed in both the GDSV and GDSV-VEGF groups. In contrast, a small amount of new bone grew around the edges of the defects in the GelMA and GelMA-VEGF groups and no obvious new bone was formed in the control group. Quantified analyses of BV/TV and BMD (Fig. 6B) indicated that the GDSV-VEGF group promoted the highest volume of new bone formation which was distinctly greater than that of the GDSV group and the other three groups. Interestingly, although the amount of new bone formed in the GDSV group was lower than that in the GDSV-VEGF group, the new bone volume was still significantly higher than that in the other groups.

In addition, undecalcified sections stained with VG were used to further evaluate the bone regenerative effects of the hydrogels. As shown in Fig. 6C and D, new bone tissues were observed more in the GDSV (35.62 ± 2.32 %) and GDSV-VEGF (46.82 ± 2.01 %) groups, and the GDSV-VEGF group exhibited the highest new bone formation in the defect area. In contrast, less regenerated bone was observed in the

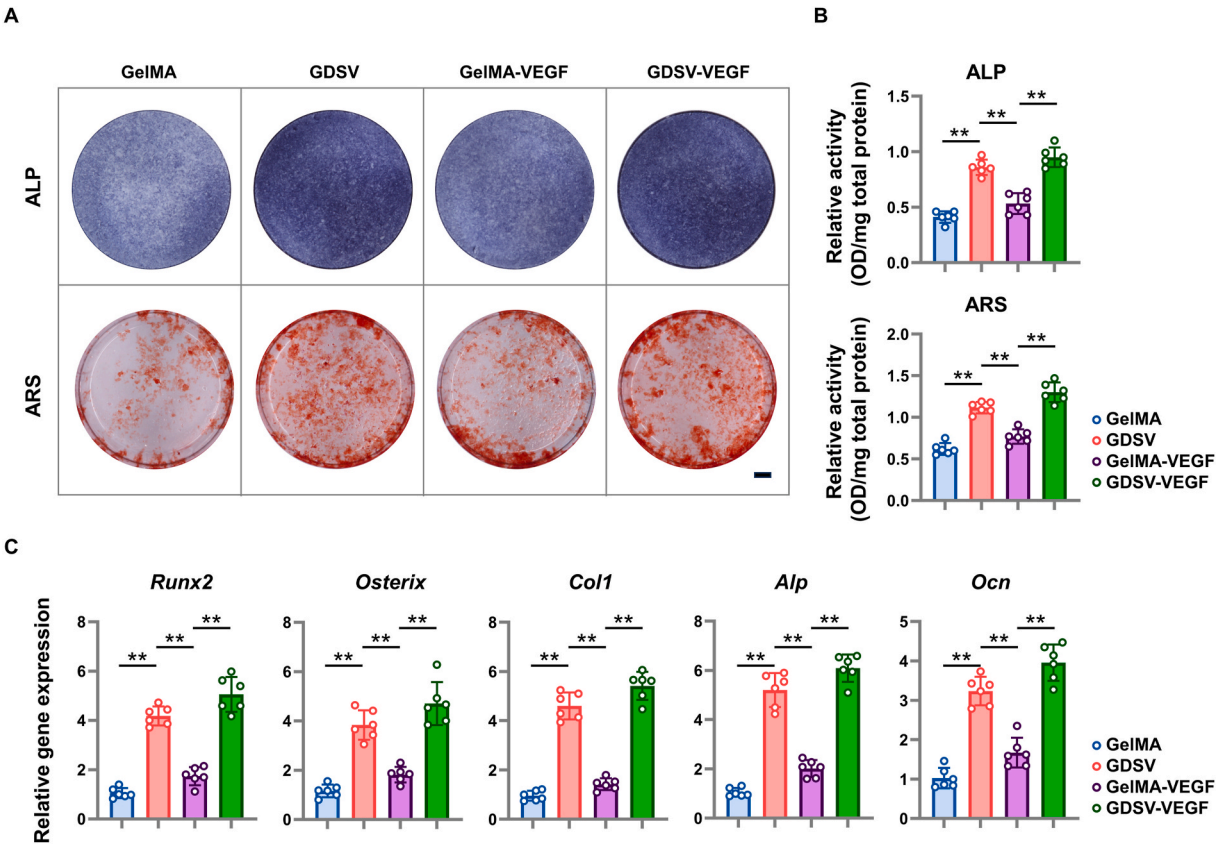

Fig. 5. GDSV hydrogel for enhancing BMSCs osteogenic differentiation *in vitro*. A) ALP and ARS staining of BMSCs on GelMA, GelMA-VEGF, GDSV and GDSV-VEGF hydrogels, scale bar = 1 mm. B) Semi-quantitative analysis of ALP and ARS activity (n = 6, $^{**}p < 0.01$). C) Expression of osteogenic-related genes (*Runx2*, *Osterix*, *Col1*, *Alp*, and *Ocn*) in BMSCs on different hydrogels (n = 6, $^{**}p < 0.01$).

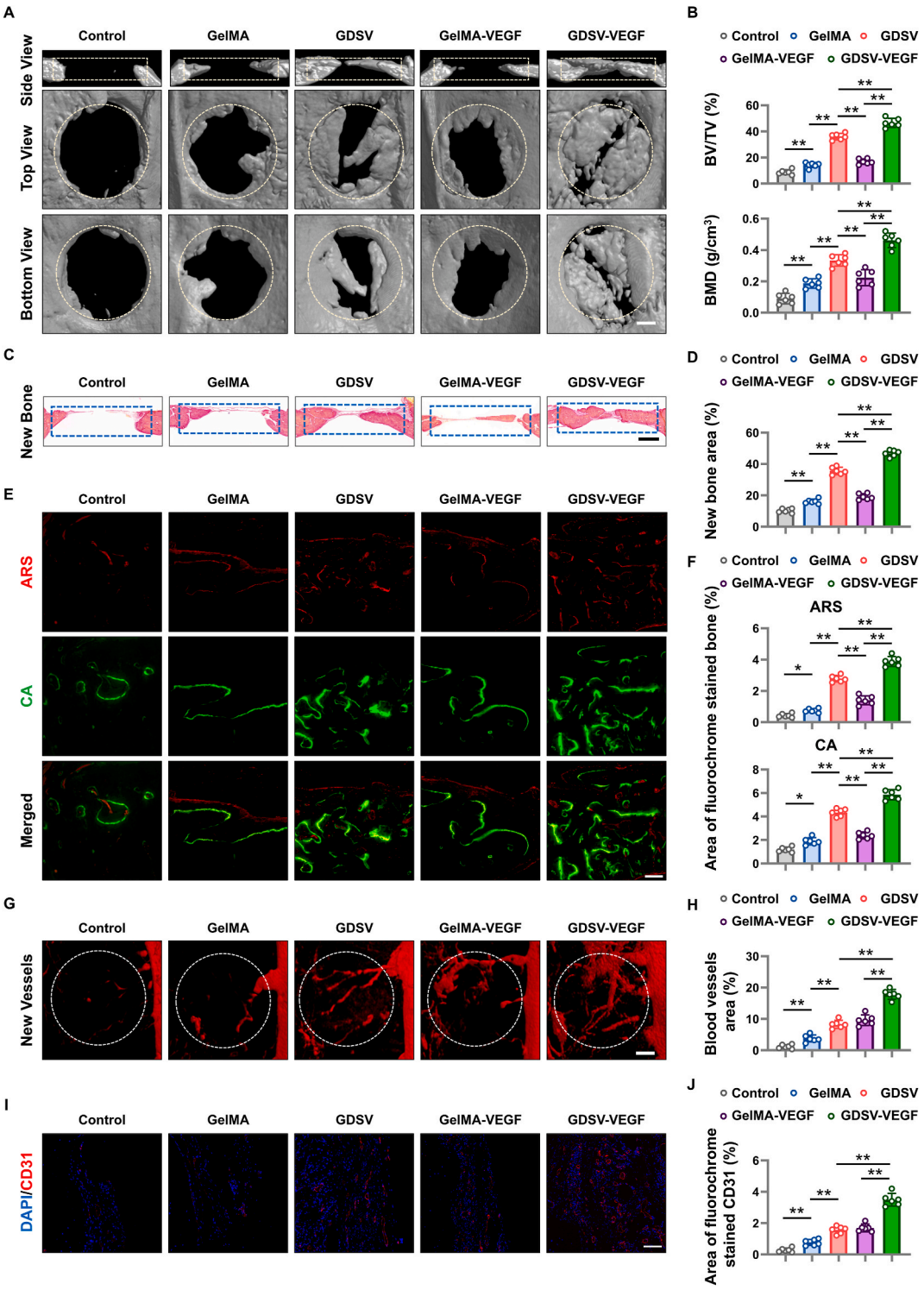

Fig. 6. GDSV-VEGF hydrogel for promoting vascularized bone formation *in vivo*. A) Micro-CT reconstruction of cranium defects implanted with different hydrogels (Groups: control, GelMA, GDSV, GelMA-VEGF, and GDSV-VEGF) 8 weeks after the operation. The new bone formation in the defect regions (indicated by white rectangle or circle) was observed from side view, top view and bottom view, control group: cranium defects without hydrogel, scale bar = 1 mm. B) Quantitative analysis of BV/TV and BMD (n = 6, $^{**}p < 0.01$). C) Undecalcified sections with VG staining were performed to observe new bone formation in the defect regions (indicated by blue rectangle) as histological evaluation, scale bar = 1 mm. D) Quantitative analysis of new bone area (n = 6, $^{**}p < 0.01$). E) Sequential fluorescent labeling for dynamic bone mineralization by ARS, (red, 4 weeks) and CA (green, 6 weeks), scale bar = 100 μm. F) Quantitative analysis of ARS and CA labelled area (n = 6, $^{*}p < 0.05$, $^{**}p < 0.01$). G) Micro-CT reconstruction of new blood vessels perfused with Microfil in defect areas (indicated by white circle) 8 weeks after the operation, scale bar = 1 mm. H) Quantitative analysis of new blood vessels area (n = 6, $^{**}p < 0.01$). I) Decalcified sections with immunofluorescent staining of CD31 were performed to observe new vessels formation (CD31: red, cell nuclei: blue), scale bar = 100 μm. J) Quantitative analysis of CD31 labelled area (n = 6, $^{**}p < 0.01$).

GelMA and GelMA-VEGF groups and large areas of the defects were filled with fibrous connective tissues. Similar results were observed in the Masson's trichrome staining (Figs. S5A and B), the new bone collagen fibers (blue) were observed more in the GDSV (31.76 ± 2.65 %) and GDSV-VEGF (44.01 ± 2.45 %) groups, and the GDSV-VEGF group exhibited the highest new bone formation in the defect area. Sequential fluorescent labeling analysis was performed to monitor dynamic bone mineralization (Fig. 6E). At 4 weeks, the percentage of the ARS-labelled area (red) in the GDSV-VEGF group was the highest among all groups. A similar trend was observed in the CA-labelled area (green) at 6 weeks; the GDSV-VEGF group had the largest positive-labelled area. As shown in Fig. 6F, the quantitative results confirmed this trend, demonstrating that the GDSV-VEGF group promoted the highest rate of mineralization and the GDSV group significantly accelerated mineral deposition, in contrast to the GelMA and GelMA-VEGF groups. These new bone formation results indicated that the GDSV hydrogel could provide basic mechanical support, and its dynamic ECM characteristic of stress relaxation promoted the endogenous stem cells recruited by Apt19S for

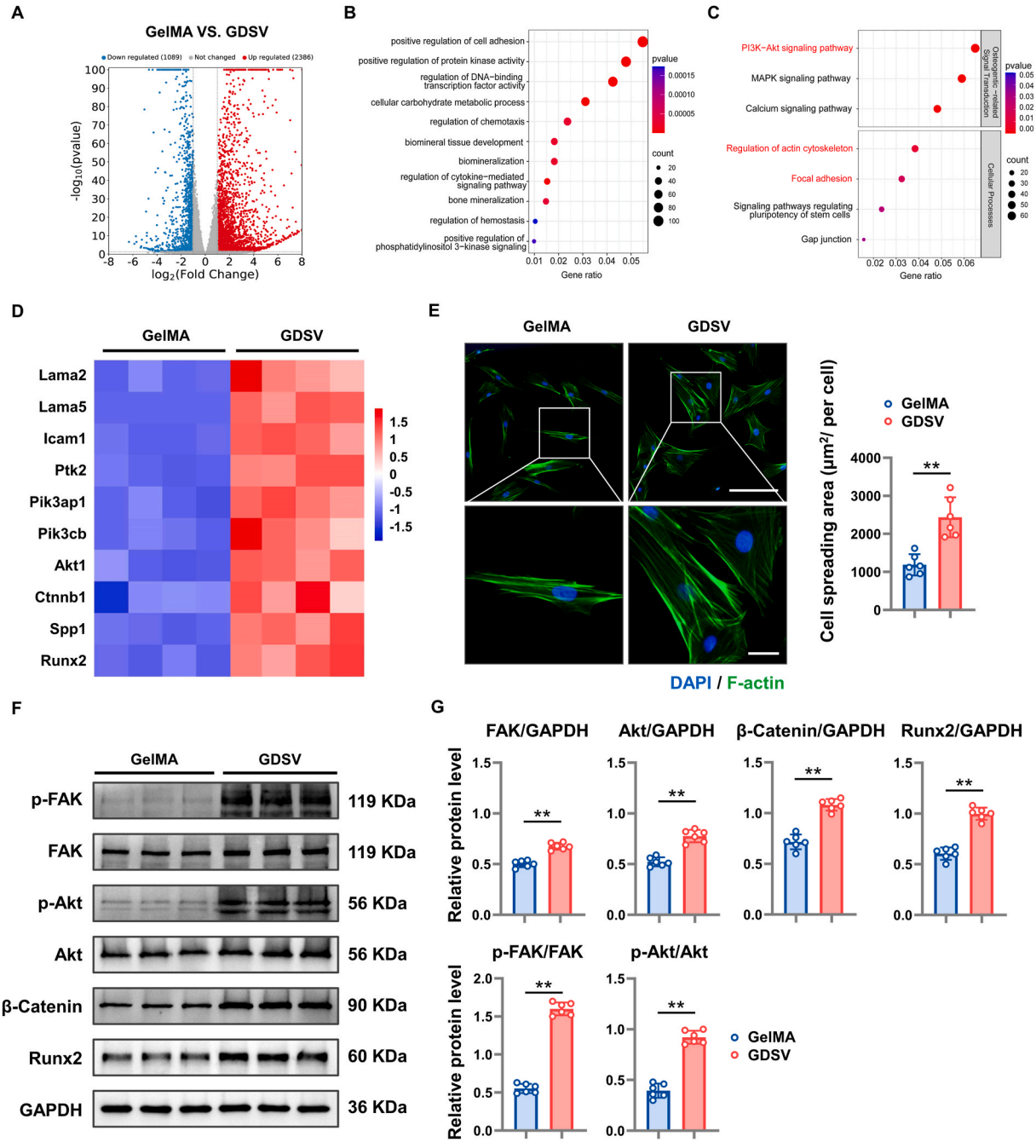

Fig. 7. Mechanism and role of GDSV hydrogel for promoting BMSCs osteogenic differentiation. A) Volcano diagram of DEGs between GelMA and GDSV groups. B) Gene enrichment GO-BP (Biological process) analysis of GDSV group *vs.* GelMA group. C) Gene enrichment KEGG pathways analysis of GDSV group *vs.* GelMA group. D) Heat map of DEGs related to cell adhesion and osteogenesis in GDSV group *vs.* GelMA group, such as Ptk2 encoding FAK, Ctnnb1 encoding β-Catenin (n = 4). E) Immunofluorescent staining of F-actin to observe BMSCs adhesion on different hydrogels (F-actin: green, cell nuclei: blue), scale bar = 100 μm and 20 μm, quantitative analysis of cell spreading area (n = 6, $^{**}p < 0.01$). F) Western blot analysis of protein expression of FAK, p-FAK, Akt, p-Akt, β-Catenin, Runx2 and GAPDH between GelMA and GDSV groups. G) Quantitative analysis of FAK, Akt, β-Catenin, Runx2 normalized to GAPDH, p-FAK normalized to FAK, and p-Akt normalized to Akt (n = 6, $^{**}p < 0.01$).

osteogenic differentiation, which resulted in the promotion of new bone growth.

Regarding neovascularization, radiographic and histological analyses were performed to evaluate the angiogenic potential of different hydrogels *in vivo*. As shown in Fig. 6G, in the GDSV-VEGF group, remarkable blood vessel growth was observed in the central regions of the defects (indicated by white circles). By contrast, only a few blood vessels appeared in the GelMA and GelMA-VEGF groups, and these vessels were mainly distributed at the edges of the defects. Notably, in the GDSV group, some blood vessels were observed in the central areas of the defects, but were fewer than those in the GDSV-VEGF group. We quantified the perfused blood vessels with 3D reconstruction (Fig. 6H), and the results suggested that the GDSV-VEGF group (17.84 ± 1.54 %) induced the highest new blood vessel area among all groups. Moreover, CD31 immunofluorescence staining was performed to assess vascularization from a histological perspective. As shown in Fig. 6I, the GDSV-VEGF group displayed larger areas of positive stained capillaries (red, 3.49 ± 0.4 %) than the other groups, and the quantitative analyses (Fig. 6J) were consistent with the observation, indicating that the GDSV-VEGF hydrogel possesses a considerable potential to promote vascularization *in vivo*.

Overall, the GDSV-VEGF hydrogel showed a superior capacity to enhance osteogenesis and angiogenesis, thereby promoting vascularized bone formation. Notably, the GDSV hydrogel could accelerate the differentiation of BMSCs towards the osteogenic line positively, and regenerate more new bone tissue compared to the GelMA hydrogels with or without VEGF. This suggested that the GDSV hydrogel could provide physiological cues to stimulate BMSCs towards osteogenic differentiation. In addition, the optimum effect on vascularized bone regeneration was detected in the GDSV-VEGF group, which may be due to the fact that VEGF stimulates the formation of new vascular networks via endothelial cells. Based on this evidence, we propose that the GDSV-VEGF hydrogel enhances vascularized bone regeneration by gradually releasing VEGF throughout the process. Hence, it is convinced that the GDSV hydrogel loaded with VEGF contributes to the synergistic effect on promoting vascularized bone regeneration.

3.7. Mechanism and role of GDSV hydrogel for promoting BMSCs osteogenic differentiation

Because both *in vitro* and *in vivo* results indicated that the GDSV hydrogel could significantly enhance osteogenesis compared with the GelMA hydrogel, the underlying molecular mechanism was also detected via a series of tests. According to the RNA-seq results, volcano plots showed 2386 up-regulated and 1089 down-regulated genes in the GDSV *vs*. GelMA plot (Fig. 7A). GO analysis indicated that the up-regulated DEGs in the GDSV group were primarily associated with the biological process (BP) of cell adhesion, protein kinase activity, biomineral tissue development, and bone mineralization (Fig. 7B). As shown in Fig. 7C, KEGG analysis showed that GDSV activated cellular processes related to the actin cytoskeleton and focal adhesion. In addition, several osteogenic-related signal transductions pathways, especially the phosphatidylinositol 3-kinase/protein kinase B (PI3K/Akt) signaling pathway, were notably up-regulated in the GDSV group. In addition, compared with the GelMA group, DEGs involved in cell adhesion and osteogenesis were significantly up-regulated in the GDSV group (Fig. 7D). Whole RNA-seq analyses indicated that cell adhesion and mechanical signal transduction played critical roles in promoting the osteogenic differentiation of BMSCs in the GDSV group. Immunofluorescence staining of F-actin was performed to observe cell adhesion on different hydrogels. As shown in Fig. 7E, BMSCs cultured on GDSV extended more widely and exhibited larger spreading areas than cells cultured on GelMA, indicating that GDSV with stress relaxation could positively regulate the cytoskeleton and promote cell adhesion. Moreover, Western blot was performed to further detect the osteogenic molecular mechanism at the protein level. As shown in Fig. 7F and G, compared to the GelMA group, both the total and phosphorylated levels of FAK and Akt were significantly up-regulated in the GDSV group. Besides, the protein expression of β-Catenin and Runx2 increased considerably in the GDSV group.

These results indicated that, compared with the GelMA group, a series of biological processes and signaling pathways related to cell adhesion and osteogenesis were significantly affected in the GDSV group. For instance, RNA-seq analyses showed a positive regulation of cell adhesion, which was consistent with our immunofluorescence staining results of the cytoskeleton on different hydrogels. In our results, the BMSCs spread over larger areas of F-actin on the GDSV hydrogel, indicating that a substrate with rapid stress relaxation could facilitate the spreading and adhesion of cells, which has been proven in previous studies [61]. In addition, according to the enrichment pathways of focal adhesion and the biological process of the positive regulation of protein kinase activity, we detected FAK expression via western blot. Both the total FAK and p-FAK expression were significantly up-regulated in the GDSV group. As a key role in the focal adhesion core, FAK can transmit extracellular signals into inner signaling cascades [62]. The high expression of FAK further indicated that the GDSV hydrogel with rapid stress relaxation provided significant mechanical cues to stimulate focal adhesion activity, thereby affecting intracellular signal transduction.

When detecting intracellular signaling pathways, we observed that a large number of DEGs were enriched in the PI3K/Akt signaling pathway. As a key intracellular signaling pathway that regulates cell biological behaviors such as cell survival, proliferation, and differentiation, the PI3K/Akt signaling pathway has been proven to be a critical downstream signaling of focal adhesion and is able to transduce mechanical signals [63]. We tested the protein expression of Akt, and found that p-Akt expression was significantly up-regulated in the GDSV group. Previous reports have shown that the PI3K/Akt signaling pathway is capable of receiving upstream signals from focal adhesions, and that phosphorylation of the PI3K/Akt pathway triggers a change in cell behaviors [64]. Lin et al. observed that hydrogel with rapid stress relaxation could promote cell proliferation via the PI3K/Akt signaling pathway, which is consistent with our results of the cell proliferation test [65].

Although the PI3K/Akt signaling pathway is a key regulator of bone formation, the definite role of this pathway in promoting cell osteogenic differentiation has not been clarified. The classical Wnt/β-Catenin pathway can regulate cell functions via stabilizing the β-Catenin level and promoting its subcellular localization. In bone repair, β-Catenin can translocate to the nucleus and activate the transcription of a wide range of downstream osteogenic-related genes directly [66,67]. Recent studies demonstrated the crosstalk between the PI3K/Akt and Wnt/β-Catenin pathways in regulating osteogenesis [68,69].

In other words, phosphorylated Akt has been proven to maintain the accumulation of β-Catenin, and PI3K/Akt/β-Catenin axis regulating cell osteogenic differentiation and mineralization occurs. In our results, the Ctnnb1 gene, which encodes β-Catenin, was expressed significantly different between the GelMA and GDSV groups. Moreover, the protein expression of β-Catenin and Runx2 was noticeably up-regulated in the GDSV group, indicating that β-Catenin played a crucial role in the process of GDSV promoting osteogenic differentiation. Interestingly, because the KEGG pathways results showed no significant difference in the enrichment of genes related to the classical Wnt pathway, the up-regulation of β-Catenin was attributed to the activation of PI3K/Akt rather than the canonical Wnt pathway. The above results demonstrated that the GDSV hydrogel with rapid stress relaxation could modify the cytoskeleton and facilitate cell adhesion, and the mechanical cues could promote BMSCs osteogenic differentiation via a FAK/PI3K/Akt/β-Catenin axis.

4. Conclusion

In summary, we have successfully developed a composite hydrogel

comprising GelMA and DNA decorated with aptamers. This hydrogel demonstrates the combined advantages of rapid stress relaxation that is similar to viscoelastic ECM, and multiple functionalities that enhance vascularized bone formation. Our results indicated that the GDSV-VEGF hydrogel could sustainably release VEGF and promote angiogenesis. Furthermore, the GDSV hydrogel has the ability to promote osteogenesis and enhance the osteogenic differentiation of BMSCs by facilitating cell adhesion and activating the FAK/PI3K/Akt/β-Catenin signaling pathway. Overall, our findings suggest that this composite hydrogel, based on aptamer-modified DNA backbones with biological properties resembling those of natural bone ECM, is a promising biomaterial for bone repair.

Ethics approval and consent to participate

All the animal procedures were reviewed and approved by the Institutional Animal Care and Use Committee of Renji Hospital, Shanghai Jiao Tong University School of Medicine. The animal license number is RJ2022-1004.

CRediT authorship contribution statement

Guanglong Li: Writing – original draft, Methodology, Investigation, Funding acquisition, Conceptualization. **Fei Gao:** Resources, Methodology, Investigation, Funding acquisition. **Donglei Yang:** Writing – review & editing, Resources, Methodology, Data curation. **Lu Lin:** Writing – review & editing, Methodology, Investigation. **Weijun Yu:** Writing – review & editing, Methodology, Investigation. **Jiaqi Tang:** Writing – review & editing, Methodology, Investigation. **Ruhan Yang:** Writing – review & editing, Methodology, Investigation. **Min Jin:** Writing – review & editing, Validation, Supervision, Funding acquisition, Formal analysis. **Yuting Gu:** Writing – review & editing, Supervision, Methodology, Formal analysis. **Pengfei Wang:** Writing – original draft, Validation, Supervision, Project administration, Data curation, Conceptualization. **Eryi Lu:** Writing – original draft, Validation, Supervision, Project administration, Funding acquisition, Conceptualization.

Declaration of competing interest

The authors declare that they have no known competing financial interests or personal relationships that could have appeared to influence the work reported in this paper.

Acknowledgements

This work was supported by National Natural Science Foundation of China (Grant Nos. 52171075, 52103172, 82271589), Science and Technology Commission of Shanghai Municipality (Grant Nos. 21DZ2294700, 21ZR1439400), Opening Project of Shanghai Key Laboratory of Orthopaedic Implant (Grant No. KFKT2021001), the Nonprofit Central Research Institute Fund of Chinese Academy of Medical Sciences (Grant No. 2023-JKCS-14), Incubating Program for National Program of Renji Hospital, Shanghai Jiao Tong University School of Medicine (Grant No. RJTJ23-PY-053), and "Clinic Plus" Outstanding Project of Shanghai Key Laboratory for Nucleic Acid Chemistry and Nanomedicine (Grant No. 2021ZYA009).

Appendix A. Supplementary data

Supplementary data to this article can be found online at https://doi.org/10.1016/j.bioactmat.2024.08.035.

References

[1] W. Wang, K.W.K. Yeung, Bone grafts and biomaterials substitutes for bone defect repair: a review, Bioact. Mater. 2 (2017) 224–247, https://doi.org/10.1016/j.bioactmat.2017.05.007.
[2] S. Pina, J.M. Oliveira, R.L. Reis, Natural-based nanocomposites for bone tissue engineering and regenerative medicine: a review, Adv. Mater. 27 (2015) 1143–1169, https://doi.org/10.1002/adma.201403354.
[3] A. Kumar, K.M. Rao, S.S. Han, Synthesis of mechanically stiff and bioactive hybrid hydrogels for bone tissue engineering applications, Chem. Eng. J. 317 (2017) 119–131, https://doi.org/10.1016/j.cej.2017.02.065.
[4] E.-J. Lee, M. Jain, S. Alimperti, Bone microvasculature: stimulus for tissue function and regeneration, Tissue Eng. Part B Rev. 27 (2021) 313–329, https://doi.org/10.1089/ten.TEB.2020.0154.
[5] A. Marrella, T.Y. Lee, D.H. Lee, S. Karuthedom, D. Syla, A. Chawla, A. Khademhosseini, H.L. Jang, Engineering vascularized and innervated bone biomaterials for improved skeletal tissue regeneration, Mater, Today Off. 21 (2018) 362–376, https://doi.org/10.1016/j.mattod.2017.10.005.
[6] K. Liu, L. Li, J. Chen, Y. Li, W. Wen, L. Lu, L. Li, H. Li, M. Liu, C. Zhou, B. Luo, Bone ECM-like 3D printing scaffold with liquid crystalline and viscoelastic microenvironment for bone regeneration, ACS Nano 16 (2022) 21020–21035, https://doi.org/10.1021/acsnano.2c08699.
[7] J.M. Aamodt, D.W. Grainger, Extracellular matrix-based biomaterial scaffolds and the host response, Biomaterials 86 (2016) 68–82, https://doi.org/10.1016/j.biomaterials.2016.02.003.
[8] O. Chaudhuri, L. Gu, D. Klumpers, M. Darnell, S.A. Bencherif, J.C. Weaver, N. Huebsch, H.-P. Lee, E. Lippens, G.N. Duda, D.J. Mooney, Hydrogels with tunable stress relaxation regulate stem cell fate and activity, Nat. Mater. 15 (2016) 326–334, https://doi.org/10.1038/nmat4489.
[9] O. Chaudhuri, J. Cooper-White, P.A. Janmey, D.J. Mooney, V.B. Shenoy, Effects of extracellular matrix viscoelasticity on cellular behaviour, Nature 584 (2020) 535–546, https://doi.org/10.1038/s41586-020-2612-2.
[10] J. Whitehead, K.H. Griffin, M. Gionet-Gonzales, C.E. Vorwald, S.E. Cinque, J. K. Leach, Hydrogel mechanics are a key driver of bone formation by mesenchymal stromal cell spheroids, Biomaterials 269 (2021) 120607, https://doi.org/10.1016/j.biomaterials.2020.120607.
[11] M.M. Martino, P.S. Briquez, K. Maruyama, J.A. Hubbell, Extracellular matrix-inspired growth factor delivery systems for bone regeneration, Adv. Drug Deliv. Rev. 94 (2015) 41–52, https://doi.org/10.1016/j.addr.2015.04.007.
[12] P. Tayalia, D.J. Mooney, Controlled growth factor delivery for tissue engineering, Adv. Mater. 21 (2009) 3269–3285, https://doi.org/10.1002/adma.200900241.
[13] B.-H. Shan, F.-G. Wu, Hydrogel-based growth factor delivery platforms: strategies and recent advances, Adv. Mater. 36 (2023) 2210707, https://doi.org/10.1002/adma.202210707.
[14] D. Seliktar, Designing cell-compatible hydrogels for biomedical applications, Science 336 (2012) 1124–1128, https://doi.org/10.1126/science.1214804.
[15] Z.-K. Cui, S. Kim, J.J. Baljon, B.M. Wu, T. Aghaloo, M. Lee, Microporous methacrylated glycol chitosan-montmorillonite nanocomposite hydrogel for bone tissue engineering, Nat. Commun. 10 (2019) 3523, https://doi.org/10.1038/s41467-019-11511-3.
[16] X. Xue, Y. Hu, S. Wang, X. Chen, Y. Jiang, J. Su, Fabrication of physical and chemical crosslinked hydrogels for bone tissue engineering, Bioact. Mater. 12 (2022) 327–339, https://doi.org/10.1016/j.bioactmat.2021.10.029.
[17] F.K. Lewns, O. Tsigkou, L.R. Cox, R.D. Wildman, L.M. Grover, G. Poologasundarampillai, Hydrogels and bioprinting in bone tissue engineering: creating artificial stem-cell niches for in vitro models, Adv. Mater. 35 (2023) e2301670, https://doi.org/10.1002/adma.202301670.
[18] S.C. Neves, L. Moroni, C.C. Barrias, P.L. Granja, Leveling up hydrogels: hybrid systems in tissue engineering, Trends Biotechnol. 38 (2020) 292–315, https://doi.org/10.1016/j.tibtech.2019.09.004.
[19] K. Yue, G. Trujillo-de Santiago, M.M. Alvarez, A. Tamayol, N. Annabi, A. Khademhosseini, Synthesis, properties, and biomedical applications of gelatin methacryloyl (GelMA) hydrogels, Biomaterials 73 (2015) 254–271, https://doi.org/10.1016/j.biomaterials.2015.08.045.
[20] A.G. Kurian, R.K. Singh, K.D. Patel, J.-H. Lee, H.-W. Kim, Multifunctional GelMA platforms with nanomaterials for advanced tissue therapeutics, Bioact. Mater. 8 (2022) 267–295, https://doi.org/10.1016/j.bioactmat.2021.06.027.
[21] W. Li, W. Miao, Y. Liu, T. Wang, Y. Zhang, W. Wang, D. Lu, X. Zhou, X. Jiao, X. Jia, Y. Lin, Y. Li, H. He, Y. Mao, Z. Ma, T. Li, J. Wang, Bioprinted constructs that mimic the ossification center microenvironment for targeted innervation in bone regeneration, Adv. Funct. Mater. 32 (2022) 2109871, https://doi.org/10.1002/adfm.202109871.
[22] C.M. Madl, S.C. Heilshorn, H.M. Blau, Bioengineering strategies to accelerate stem cell therapeutics, Nature 557 (2018) 335–342, https://doi.org/10.1038/s41586-018-0089-z.
[23] K.H. Vining, D.J. Mooney, Mechanical forces direct stem cell behaviour in development and regeneration, Nat. Rev. Mol. Cell Biol. 18 (2017) 728–742, https://doi.org/10.1038/nrm.2017.108.
[24] X. Zhao, S. Liu, L. Yildirimer, H. Zhao, R. Ding, H. Wang, W. Cui, D. Weitz, Microfluidics-assisted osteogenesis: injectable stem cell-laden photocrosslinkable microspheres fabricated using microfluidics for rapid generation of osteogenic tissue constructs, Adv. Funct. Mater. 26 (2016) 2976, https://doi.org/10.1002/adfm.201670110, 2976.
[25] T.C. Lai, J. Yu, W.B. Tsai, Gelatin methacrylate/carboxybetaine methacrylate hydrogels with tunable crosslinking for controlled drug release, J. Mater. Chem. B 4 (2016) 2304–2313, https://doi.org/10.1039/c5tb02518d.

[26] T. Xin, J. Mao, L. Liu, J. Tang, L. Wu, X. Yu, Y. Gu, W. Cui, L. Chen, Programmed sustained release of recombinant human bone morphogenetic protein-2 and inorganic ion composite hydrogel as artificial periosteum, ACS Appl. Mater. Interfaces 12 (2020) 6840–6851, https://doi.org/10.1021/acsami.9b18496.
[27] Y. Shao, H. Jia, T. Cao, D. Liu, Supramolecular hydrogels based on DNA self-assembly, Acc. Chem. Res. 50 (2017) 659–668, https://doi.org/10.1021/acs.accounts.6b00524.
[28] B. Yang, B. Zhou, C. Li, X. Li, Z. Shi, Y. Li, C. Zhu, X. Li, Y. Hua, Y. Pan, J. He, T. Cao, Y. Sun, W. Liu, M. Ge, Y.R. Yang, Y. Dong, D. Liu, A biostable l-DNA hydrogel with improved stability for biomedical applications, Angew. Chem., Int. Ed. Engl. 61 (2022) e202202520, https://doi.org/10.1002/anie.202202520.
[29] L. Wu, Y. Wang, X. Xu, Y. Liu, B. Lin, M. Zhang, J. Zhang, S. Wan, C. Yang, W. Tan, Aptamer-based detection of circulating targets for precision medicine, Chem. Rev. 121 (2021) 12035–12105, https://doi.org/10.1021/acs.chemrev.0c01140.
[30] M. Vázquez-González, I. Willner, Aptamer-functionalized hybrid nanostructures for sensing, drug delivery, catalysis and mechanical applications, Int. J. Mol. Sci. 22 (2021) 1803, https://doi.org/10.3390/ijms22041803.
[31] X. Hu, Y. Wang, Y. Tan, J. Wang, H. Liu, Y. Wang, S. Yang, M. Shi, S. Zhao, Y. Zhang, Q. Yuan, A difunctional regeneration scaffold for knee repair based on aptamer-directed cell recruitment, Adv. Mater. 29 (2017), https://doi.org/10.1002/adma.201605235.
[32] X. Zhang, Q. Li, L. Li, J. Ouyang, T. Wang, J. Chen, X. Hu, Y. Ao, D. Qin, L. Zhang, J. Xue, J. Cheng, W. Tao, Bioinspired mild photothermal effect-reinforced multifunctional fiber scaffolds promote bone regeneration, ACS Nano 17 (2023) 6466–6479, https://doi.org/10.1021/acsnano.2c11486.
[33] J. Son, J. Kim, K. Lee, J. Hwang, Y. Choi, Y. Seo, H. Jeon, H.C. Kang, H.-M. Woo, B.-J. Kang, J. Choi, DNA aptamer immobilized hydroxyapatite for enhancing angiogenesis and bone regeneration, Acta Biomater. 99 (2019) 469–478, https://doi.org/10.1016/j.actbio.2019.08.047.
[34] A. Stejskalová, N. Oliva, F.J. England, B.D. Almquist, Biologically inspired, cell-selective release of aptamer-trapped growth factors by traction forces, Adv. Mater. 31 (2019) e1806380, https://doi.org/10.1002/adma.201806380.
[35] T. Yuan, Y. Shao, X. Zhou, Q. Liu, Z. Zhu, B. Zhou, Y. Dong, N. Stephanopoulos, S. Gui, H. Yan, D. Liu, Highly permeable DNA supramolecular hydrogel promotes neurogenesis and functional recovery after completely transected spinal cord injury, Adv. Mater. 33 (2021) e2102428, https://doi.org/10.1002/adma.202102428.
[36] W. Ma, Y. Zhan, Y. Zhang, C. Mao, X. Xie, Y. Lin, The biological applications of DNA nanomaterials: current challenges and future directions, Signal Transduct Target, Ther 6 (2021) 351, https://doi.org/10.1038/s41392-021-00727-9.
[37] Y. Miao, Y. Chen, J. Luo, X. Liu, Q. Yang, X. Shi, Y. Wang, Black phosphorus nanosheets-enabled DNA hydrogel integrating 3D-printed scaffold for promoting vascularized bone regeneration, Bioact. Mater. 21 (2023) 97–109, https://doi.org/10.1016/j.bioactmat.2022.08.005.
[38] Q. Yang, Y. Miao, J. Luo, Y. Chen, Y. Wang, Amyloid fibril and clay nanosheet dual-nanoengineered DNA dynamic hydrogel for vascularized bone regeneration, ACS Nano 17 (2023) 17131–17147, https://doi.org/10.1021/acsnano.3c04816.
[39] D. Athanasiadou, N. Meshry, N.G. Monteiro, A.C. Ervolino-Silva, R.L. Chan, C. A. McCulloch, R. Okamoto, K.M.M. Carneiro, DNA hydrogels for bone regeneration, Proc. Natl. Acad. Sci. U.S.A. 120 (2023) e2220565120, https://doi.org/10.1073/pnas.2220565120.
[40] Y. Dong, C. Yao, Y. Zhu, L. Yang, D. Luo, D. Yang, DNA functional materials assembled from branched DNA: design, synthesis, and applications, Chem. Rev. 120 (2020) 9420–9481, https://doi.org/10.1021/acs.chemrev.0c00294.
[41] H. Jiang, V. Pan, S. Vivek, E.R. Weeks, Y. Ke, Programmable DNA hydrogels assembled from multidomain DNA strands, Chembiochem 17 (2016) 1156–1162, https://doi.org/10.1002/cbic.201500686.
[42] F. Gao, Z. Xu, Q. Liang, H. Li, L. Peng, M. Wu, X. Zhao, X. Cui, C. Ruan, W. Liu, Osteochondral regeneration with 3D-printed biodegradable high-strength supramolecular polymer reinforced-gelatin hydrogel scaffolds, Adv. Sci. 6 (2019) 1900867, https://doi.org/10.1002/advs.201900867.
[43] S. Li, C. Song, S. Yang, W. Yu, W. Zhang, G. Zhang, Z. Xi, E. Lu, Supercritical CO2 foamed composite scaffolds incorporating bioactive lipids promote vascularized bone regeneration via Hif-1α upregulation and enhanced type H vessel formation, Acta, Biomater 94 (2019) 253–267, https://doi.org/10.1016/j.actbio.2019.05.066.
[44] Q. Chen, S. Wang, T. Huang, F. Xiao, Z. Wu, R. Yu, Construction and research of multiple stimuli-responsive 2D photonic crystal DNA hydrogel sensing platform with double-network structure and signal self-expression, Anal. Chem. 94 (2022) 5530–5537, https://doi.org/10.1021/acs.analchem.1c04390.
[45] M. Bansal, B. Raos, Z. Aqrawe, Z. Wu, D. Svirskis, An interpenetrating and patternable conducting polymer hydrogel for electrically stimulated release of glutamate, Acta, Biomater 137 (2022) 124–135, https://doi.org/10.1016/j.actbio.2021.10.010.
[46] E.O. Shatabayeva, D.B. Kaldybekov, L. Ulmanova, B.A. Zhaisanbayeva, E.A. Mun, Z.A. Kenessova, S.E. Kudaibergenov, V.V. Khutoryanskiy, Enhancing mucoadhesive properties of gelatin through chemical modification with unsaturated anhydrides, Biomacromolecules 25 (2024) 1612–1628, https://doi.org/10.1021/acs.biomac.3c01183.
[47] P. Kolar, K. Schmidt-Bleek, H. Schell, T. Gaber, D. Toben, G. Schmidmaier, C. Perka, F. Buttgereit, G.N. Duda, The early fracture hematoma and its potential role in fracture healing, Tissue Eng. Part B Rev. 16 (2010) 427–434, https://doi.org/10.1089/ten.TEB.2009.0687.
[48] M. Darnell, S. Young, L. Gu, N. Shah, E. Lippens, J. Weaver, G. Duda, D. Mooney, Substrate stress-relaxation regulates scaffold remodeling and bone formation in vivo, Adv. Healthcare Mater. 6 (2017), https://doi.org/10.1002/adhm.201601185, 10.1002/adhm.201601185.
[49] H. Wang, S.C. Heilshorn, Adaptable hydrogel networks with reversible linkages for tissue engineering, Adv. Mater. 27 (2015) 3717–3736, https://doi.org/10.1002/adma.201501558.
[50] Z. Tong, L. Jin, J.M. Oliveira, R.L. Reis, Q. Zhong, Z. Mao, C. Gao, Adaptable hydrogel with reversible linkages for regenerative medicine: dynamic mechanical microenvironment for cells, Bioact, Mater 6 (2021) 1375–1387, https://doi.org/10.1016/j.bioactmat.2020.10.029.
[51] Y.H. Peng, S.K. Hsiao, K. Gupta, A. Ruland, G.K. Auernhammer, M.F. Maitz, S. Boye, J. Lattner, C. Gerri, A. Honigmann, C. Werner, E. Krieg, Dynamic matrices with DNA-encoded viscoelasticity for cell and organoid culture, Nat. Nanotechnol. 18 (2023) 1463–1473, https://doi.org/10.1038/s41565-023-01483-3.
[52] X. Xu, V.V. Jerca, R. Hoogenboom, Bioinspired double network hydrogels: from covalent double network hydrogels via hybrid double network hydrogels to physical double network hydrogels, Mater. Horiz. 8 (2021) 1173–1188, https://doi.org/10.1039/d0mh01514h.
[53] J. Kim, J. Park, G. Choe, S.-I. Jeong, H.-S. Kim, J.Y. Lee, A gelatin/alginate double network hydrogel nerve guidance conduit fabricated by a chemical-free gamma radiation for peripheral nerve regeneration, Adv. Healthcare Mater. (2024) e2400142, https://doi.org/10.1002/adhm.202400142.
[54] N. Zhao, J. Coyne, M. Xu, X. Zhang, A. Suzuki, P. Shi, J. Lai, G.-H. Fong, N. Xiong, Y. Wang, Assembly of bifunctional aptamer-fibrinogen macromer for VEGF delivery and skin wound healing, Chem. Mater. 31 (2019) 1006–1015, https://doi.org/10.1021/acs.chemmater.8b04486.
[55] D.T. Wu, M. Diba, S. Yang, B.R. Freedman, A. Elosegui-Artola, D.J. Mooney, Hydrogel viscoelasticity modulates migration and fusion of mesenchymal stem cell spheroids, Bioeng. Transl. Med. 8 (2023) e10464, https://doi.org/10.1002/btm2.10464.
[56] S. Nam, R. Stowers, J. Lou, Y. Xia, O. Chaudhuri, Varying PEG density to control stress relaxation in alginate-PEG hydrogels for 3D cell culture studies, Biomaterials 200 (2019) 15–24, https://doi.org/10.1016/j.biomaterials.2019.02.004.
[57] A. Bauer, L. Gu, B. Kwee, W.A. Li, M. Dellacherie, A.D. Celiz, D.J. Mooney, Hydrogel substrate stress-relaxation regulates the spreading and proliferation of mouse myoblasts, Acta Biomater. 62 (2017) 82–90, https://doi.org/10.1016/j.actbio.2017.08.041.
[58] H.T. Ong, R.J. Dilley, Novel non-angiogenic role for mesenchymal stem cell-derived vascular endothelial growth factor on keratinocytes during wound healing, Cytokine Growth Factor Rev. 44 (2018) 69–79, https://doi.org/10.1016/j.cytogfr.2018.11.002.
[59] T. Sun, C. Meng, Q. Ding, K. Yu, X. Zhang, W. Zhang, W. Tian, Q. Zhang, X. Guo, B. Wu, Z. Xiong, In situ bone regeneration with sequential delivery of aptamer and BMP2 from an ECM-based scaffold fabricated by cryogenic free-form extrusion, Bioact. Mater. 6 (2021) 4163–4175, https://doi.org/10.1016/j.bioactmat.2021.04.013.
[60] K. Hu, B.R. Olsen, The roles of vascular endothelial growth factor in bone repair and regeneration, Bone 91 (2016) 30–38, https://doi.org/10.1016/j.bone.2016.06.013.
[61] O. Chaudhuri, L. Gu, M. Darnell, D. Klumpers, S.A. Bencherif, J.C. Weaver, N. Huebsch, D.J. Mooney, Substrate stress relaxation regulates cell spreading, Nat. Commun. 6 (2015) 6364, https://doi.org/10.1038/ncomms7365.
[62] S.K. Mitra, D.A. Hanson, D.D. Schlaepfer, Focal adhesion kinase: in command and control of cell motility, Nat. Rev. Mol. Cell Biol. 6 (2005) 56–68, https://doi.org/10.1038/nrm1549.
[63] H. Muhammad, Y. Rais, N. Miosge, E.M. Ornan, The primary cilium as a dual sensor of mechanochemical signals in chondrocytes, Cell. Mol. Life Sci. 69 (2012) 2101–2107, https://doi.org/10.1007/s00018-011-0911-3.
[64] T.H. Cheung, T.A. Rando, Molecular regulation of stem cell quiescence, Nat. Rev. Mol. Cell Biol. 14 (2013) 329–340, https://doi.org/10.1038/nrm3591.
[65] C. Lin, Y. He, Q. Feng, K. Xu, Z. Chen, B. Tao, X. Li, Z. Xia, H. Jiang, K. Cai, Self-renewal or quiescence? Orchestrating the fate of mesenchymal stem cells by matrix viscoelasticity via PI3K/Akt-CDK1 pathway, Biomaterials 279 (2021) 121235, https://doi.org/10.1016/j.biomaterials.2021.121235.
[66] R.T. Moon, B. Bowerman, M. Boutros, N. Perrimon, The promise and perils of Wnt signaling through beta-catenin, Science 296 (2002) 1644–1646, https://doi.org/10.1126/science.1071549.
[67] S. Vermeulen, Z. Tahmasebi Birgani, P. Habibovic, Biomaterial-induced pathway modulation for bone regeneration, Biomaterials 283 (2022) 121431, https://doi.org/10.1016/j.biomaterials.2022.121431.
[68] S.-J. Zhao, F.-Q. Kong, J. Jie, Q. Li, H. Liu, A.-D. Xu, Y.-Q. Yang, B. Jiang, D.-D. Wang, Z.-Q. Zhou, P.-Y. Tang, J. Chen, Q. Wang, Z. Zhou, Q. Chen, G.-Y. Yin, H.-W. Zhang, J. Fan, Macrophage MSR1 promotes BMSC osteogenic differentiation and M2-like polarization by activating PI3K/AKT/GSK3β/β-catenin pathway, Theranostics 10 (2020) 17–35, https://doi.org/10.7150/thno.36930.
[69] B. Cai, D. Lin, Y. Li, L. Wang, J. Xie, T. Dai, F. Liu, M. Tang, L. Tian, Y. Yuan, L. Kong, S.G.F. Shen, N2-Polarized neutrophils guide bone mesenchymal stem cell recruitment and initiate bone regeneration: a missing piece of the bone regeneration puzzle, Adv. Sci. 8 (2021) e2100584, https://doi.org/10.1002/advs.202100584.